

U.S. Army Corps of Engineers
Portland District

Prototype Measurements of Pressure Fluctuations in The Dalles Dam Stilling Basin

Final Report

**Gregory R. Guensch
Marshall C. Richmond
Mark A. Weiland
Thomas J. Carlson**

March 12, 2004

Prepared by: Pacific Northwest National Laboratory
P.O. Box 999
Richland, WA 99352

**Pacific Northwest
National Laboratory**

Operated by Battelle for the
U.S. Department of Energy

DISCLAIMER

United States Government. Neither the United States Government nor any agency thereof, nor Battelle Memorial Institute, nor any of their employees, makes **any warranty, express or implied, or assumes any legal liability or responsibility for the accuracy, completeness, or usefulness of any information, apparatus, product, or process disclosed, or represents that its use would not infringe privately owned rights.** Reference herein to any specific commercial product, process, or service by trade name, trademark, manufacturer, or otherwise does not necessarily constitute or imply its endorsement, recommendation, or favoring by the United States Government or any agency thereof, or Battelle Memorial Institute. The views and opinions of authors expressed herein do not necessarily state or reflect those of the United States Government or any agency thereof.

PACIFIC NORTHWEST NATIONAL LABORATORY

operated by

BATTELLE

for the

UNITED STATES DEPARTMENT OF ENERGY

under Contract DE-AC06-76RLO1830

Printed in the United States of America

Available to DOE and DOE contractors from the
Office of Scientific and Technical Information,
P.O. Box 62, Oak Ridge, TN 37831-0062;
ph: (865) 576-8401
fax: (865) 576-5728
email: reports@adonis.osti.gov

Available to the public from the National Technical Information Service,
U.S. Department of Commerce, 5285 Port Royal Rd., Springfield, VA 22161
ph: (800) 553-6847
fax: (703) 605-6900
email: orders@ntis.fedworld.gov
online ordering: <http://www.ntis.gov/ordering.htm>



This document was printed on recycled paper.

(8/00)

Summary

Fish are believed to sustain injury at high spillway discharges from turbulence and collision with the bottom, baffle blocks and endsill in the stilling basin of The Dalles Dam, on the Columbia River. Taking velocity measurements would be exceedingly difficult in this environment, so a system of pressure transducers was installed by the Pacific Northwest National Laboratory to record high-frequency pressure data during spillway discharges. The transducers were mounted in pre-fabricated steel housings and the cable runs were held down with angle iron. The sensor housings and cable runs were bolted directly into the concrete by underwater construction divers. The transducers were mounted below spillbays 4 and 9 on the top, face, and sides of baffles; the channel between baffles; and the face and top of the endsill. Cables were run up the stilling basin to the piernose, and up the piernose and into the dam, where the data collection equipment was located. Pressure data were collected at five flow scenarios: no discharge or ambient flow conditions, discharge centered around spillbay 4 (bays 1-7), discharge centered around spillbay 9 (bays 6-12), symmetric discharge spanning the whole side of the stilling basin (bays 1-13), and an asymmetric discharge pattern spanning the whole side of the stilling basin (bays 1-14) but with higher flows around spillbay 4 (pattern recommended in biological opinion). Measured pressure data were also compared to data generated from computational fluid dynamics (CFD) model results of The Dalles Dam stilling basin.

The cable routing hardware began to fail at several locations early in the testing sequence, which limited the amount of data collected. The data obtained were processed and used to generate summary statistics and power spectra of the pressure signals. The summary statistics showed a number of expected trends such as the mean pressure increasing during head-on flow (face of baffles and endsill), decreasing in flow separation areas (top of baffles and endsill), and being proportional to depth; and the standard deviation of the pressure increasing at higher flows in all locations. The power spectra of the pressure data indicated low-frequency (1-10 Hz) energy at some locations that may have been of hydraulic origin. They also indicated significant spectral energy at higher frequencies (90-150 Hz).

Findings of the study were the following: (1) Much more robust hardware and mounting methods, bolting methods in particular, are necessary to hold equipment in the stilling basin environment, and certain regions of the stilling basin should be avoided. (2) An effective data processing approach was to bin the data into 20 equally sized sections, compute power spectra for each section, and then compute an average. (3) Static sensor data conformed in many cases to expected trends, whereas dynamic sensor data were difficult to interpret, and low-frequency (1-10 Hz) spectral peaks occurred in the pressure data at some flow patterns that may be attributable to wave action and/or turbulence. (4) Based on the mean and standard deviation of the static sensor data, the incident velocity to the endsill face was estimated to be between 15 and 25 ft/s and to fluctuate on the order of 11 ft/s about the mean. (5) Power spectra of pressure data generated with the CFD model had similar spectral shape to measured data, but frequencies of the modeled data were 0.50 to 1 order of magnitude lower due to the lower frequency at which the model data was calculated and output and the frequency inherent in the Reynolds-averaged CFD model representation of turbulence.

Acknowledgments

This project was funded by the Portland District of the United States Army Corps of Engineers under the guidance of Mike Langeslay. The rest of the staff at The Dalles Dam cooperated throughout the installation process and adjusted their operations to run the test scenarios. Lastly, RPM Construction undertook the difficult and dangerous task of installing the underwater equipment in the tailrace.

Contents

1	Introduction	1
2	Methods	3
2.1	Calibration Procedures	3
2.2	Deployment	3
2.3	Scenarios	5
2.4	Analysis	10
2.4.1	Summary Statistics	10
2.4.2	Power Spectra	11
2.4.3	Probability Density Functions	11
3	Results	13
3.1	Sensor Survival	13
3.2	Sensor Statistics	13
3.3	Power Spectra	13
3.3.1	Power Spectra Comparisons	14
3.3.2	Comparison with CFD Results	18
3.4	Probability Density Functions	18
4	Discussion	29
5	Conclusions and Recommendations	33
6	References	35
A	Spillbay Raw Data and Power Spectra	37

Figures

2.1	Overview of pressure transducer locations looking upstream	5
2.2	Schematic of sensor locations at spillbay 4, looking downstream (cable lengths in feet)	6
2.3	Schematic of sensor locations at spillbay 4, looking upstream	7
2.4	Schematic of sensor locations at spillbay 9, looking downstream (cable lengths in feet)	8
2.5	Sensor housings (Static sensor is in housing with triangular cover)	9
2.6	Dynamic sensor housing showing flush-mounted front face and protective sensor cover protruding from the back	9
2.7	Angle iron and flange used to cover cable runs, and coiled cable bundles covered with vacuum tubing	10
3.1	Comparison of ambient or static conditions versus scenario 2 results at the static sensor on the spillbay 4 sill face	20
3.2	Comparison of static or ambient conditions and scenario 2 results for the static sensor on top of the spillbay 4 endsill	21
3.3	Comparison of static versus dynamic results for the sensors on the face of the endsill below spillbay 4 during scenario 2	22
3.4	Comparison of top versus face results for the static sensors on the endsill below spillbay 4 during scenario 2	23
3.5	Comparison of results for the sill top and baffle top static sensors at spillbay 4 during scenario 2	24
3.6	Comparison of simulated and measured data on the face of the spillbay 4 endsill for scenario 2 conditions	25
3.7	Comparison of simulated and measured results at the top of the spillbay 4 endsill for scenario 2 conditions	26
3.8	Comparison of simulated and measured results at the top of the spillbay 4 baffle block for scenario 2 conditions	27
3.9	Spillbay 4, probability density plots for selected sensors and scenarios	28
4.1	Spillbay 4 at high discharge	29
4.2	Flow above baffle and endsill downstream of spillbay 4 (note the large standing wave just downstream of the endsill)	30
A.1	Static sensor data from spillbay 4	38
A.2	Power spectra of static sensor data from spillbay 4	39
A.3	Dynamic sensor data from spillbay 4	40
A.4	Power spectra of dynamic sensor data from spillbay 4	41
A.5	Static sensor data from spillbay 9	42
A.6	Power spectra of static sensor data from spillbay 9	43

Tables

2.1	Spillbay 4 calibration constants for linear expression ($V(mV) = p(psi) * a(mV/psi) + b(mV)$) where a is the coefficient and b is the offset. Note the offset, b, is zero for the dynamic sensors	3
2.2	Spillbay 9 calibration constants for linear expression ($V(mV) = p(psi) * a(mV/psi) + b(mV)$) where a is the coefficient and b is the offset. Note, the offset, b, is zero for the dynamic sensors	4
2.3	Flow scenarios in kcfs	12
3.1	Spillbay 4 sensor survival	15
3.2	Spillbay 9 sensor survival	15
3.3	Spillbay 4 sensor mean (μ) and standard deviation (σ) in ft of water for all tests (note, dynamic sensor means are near zero, and the static sensor means are similar to the sensor depth, with the exception of channel 6, which was probably malfunctioning already during the static test)	16
3.4	Spillbay 9 sensor mean (μ) and standard deviation (σ) in ft of water for all tests. Note, dynamic sensor means are near zero, and the static sensors means are similar to the sensor depth	17
3.5	Depth, mean (μ), standard deviation (σ), skewness, and kurtosis values for datasets included in this report. The skewness and kurtosis parameters reflect the normality of the data.	19

1 Introduction

The stilling basin of the spillways at The Dalles Dam Project on the Columbia River on the border of Washington and Oregon contains wedge-shaped baffles and an endsill to dissipate hydraulic energy. Fish are believed to sustain injury as a result of collision with these structures and exposure to the associated high levels of turbulence. Observational, physical model data, and computational fluid dynamics (CFD) model data suggest that strong lateral flow occurs in the stilling basin at some spill patterns, which increases the retention time of fish in the stilling basin bottom and, subsequently increases the potential for fish to collide with the structures and be exposed to severe turbulence.

The ability to characterize the hydraulic environment near the baffles and endsill in the stilling basin is extremely limited due to the high velocities and turbulent nature of the flow. One possible means of acquiring information on the flow field in such a turbulent environment is to mount pressure transducers and record pressure data. These transducers can then provide information on the mean pressures, the pressure extremes, and the variations in pressure, which can be related to velocity and turbulence.

Numerous other studies deploying pressure transducers to collect hydraulic information in turbulent environments have been conducted. Many of these have focused on tidal environments and wave action (e.g., Herbers and Guza, 1994; Elgar et al., 1995). A number of studies have also investigated wall pressure beneath boundary layers, mostly in controlled experimental environments (for a review see Bull, 1996). The studies most applicable to our situation, however, were those examining pressure fluctuations associated with hydraulic jumps (e.g., Bowers and Tsai, 1969; Toso and Bowers, 1988; Armenio et al., 2000) or submerged obstacles (e.g., Keir et al., 1969; Lauchle and Kargus, 2000). Toso and Bowers (1988) evaluated the dimensionless peak root mean square (RMS) pressure fluctuations in hydraulic jumps generated by a series of model chutes. Some of their key conclusions were that the pressure fluctuations in the jump approach a limit on the order of approximately 80 to 100% of the incident velocity head, that the pressure fluctuation distribution is not Gaussian, and that the addition of blocks and endsills did not substantially increase the magnitude of pressure fluctuations. Bowers and Tsai (1969) scaled pressure data from model studies of stilling basins up to prototype values and showed that the pressures fluctuated 40% above and below the mean pressure, and that most of the energy in the power spectrum of pressure data were at frequencies below 1 Hz. No studies were found, however, where high-frequency pressure data were collected at full scale in extremely turbulent environments such as The Dalles Dam stilling basin.

This study was conducted by the Pacific Northwest National Laboratory for the Portland District of the USACE to evaluate the feasibility of collecting pressure data at full scale in a stilling basin environment and to assess the potential of such data to contribute to fish passage improvement efforts. Specifically, the objectives of this research were the following:

1. Gain direct experience deploying instruments in an environment with such large scale turbulence
2. Evaluate the data in general terms to compare average, maximum, and minimum pressures, and the pressure variation at the various locations for each of the various scenarios, and to

infer velocity information estimates from this information

3. Determine the frequency at which various pressure phenomena occur at the various locations for the various scenarios, possibly separating out the bursting patterns, surface wave phenomena, and large- and small-scale turbulence
4. Compare the pressure information with three-dimensional hydrodynamic model results.

2 Methods

2.1 Calibration Procedures

The pressure transducer pairs consisted of a model 1502 (static) and a model 106B (dynamic) pressure sensor by PCB Piezotronics. The accuracy of the model 1502 units was 0.1% of 50 psi or 1.38 inches of water. The reported accuracy of the model 106b dynamic sensors was 1% of the full-scale pressure (8.3 psi), which converts to 2.2 inches of water.

Static sensors were calibrated by immersion to known depths in a static water column. The voltage associated with each depth was recorded. Linear regression was then used to determine the voltage to pressure relationship for that sensor. The dynamic pressure sensors had no static constant offset because they only measured pressure changes. The sensor coefficients are shown in Tables 2.1 and 2.2.

2.2 Deployment

The pressure transducers were installed downstream of spillbay 4 (Figures 2.1, 2.2 and 2.3) and spillbay 9 (Figures 2.1 and 2.4) in The Dalles Dam stilling basin. Six pairs of transducers were deployed downstream of spillbay 4 and eight pairs were deployed downstream of spillbay 9. Four transducer pairs correspond to those used in the 1:36 physical model study performed by USACE Bonneville hydraulics Laboratory. Transducer pairs were located on the front face of the baffle, the top of the baffle, the side of the baffle, the front of the end sill, the top of the end sill, and in the channel between the baffles. In the channel to the right of the baffle (looking downstream), pressure transducer pairs were mounted along the centerline in between the baffles in three locations:

Table 2.1: Spillbay 4 calibration constants for linear expression ($V(mV) = p(psi) * a(mV/psi) + b(mV)$) where a is the coefficient and b is the offset. Note the offset, b, is zero for the dynamic sensors

Channel	Sens Code	Coefficient (mV/psi)	Offset (mV)
1	SD2	314.3	
2	SS2	200.0	74.0
3	SD3	313.8	
4	SS3	200.0	85.0
5	BD1	309.2	
6	BS1	200.0	67.0
7	BD2	320.5	
8	BS2	200.0	70.0
9	BD3	323.3	
10	BS3	201.0	59.0
11	BD4	317.4	
12	BS4	200.0	85.0

Table 2.2: Spillbay 9 calibration constants for linear expression ($V(mV) = p(\text{psi}) * a(mV/\text{psi}) + b(mV)$) where a is the coefficient and b is the offset. Note, the offset, b , is zero for the dynamic sensors

Channel	Sens Code	Coefficient (mV/psi)	Offset (mV)
1	BD1	311.1	
2	BS1	201.0	79.0
3	BD2	319.9	
4	BS2	200.0	62.0
5	BD3	306.6	
6	BS3	200.0	19.0
7	BD4	308.6	
8	BS4	200.0	74.0
9	SD1	305.7	
10	SS1	200.0	97.0
11	SD2	305.0	
12	SS2	200.0	33.0
13	SD3	305.1	
14	SS3	200.0	54.0
15	SD4	317.0	
16	SS4	200.0	98.0

directly between the baffles, on the face of the end sill, and on top of the end sill.

Pressure transducers were mounted in prefabricated housings (Figures 2.5 and 2.6) and cables were bundled, covered with plastic vacuum tubing, and run under angle iron held down with prefabricated flanges (Figure 2.7). Notice that the static sensor was not flush mounted but was mounted sideways in a tent-shaped housing (Figure 2.5). This was not ideal, but it was deemed necessary because boring a hole in the concrete deep and wide enough to accommodate the length of the static sensors was not feasible, especially with the stiff cable attached to the back. The shorter dynamic sensors were flush mounted by boring a hole large enough to fit the protective pipe protruding off the back of the dynamic sensor housing (Figure 2.6). The housings and cable covers were bolted into the concrete of the piernose, stilling basin floor, baffles, and endsill by the contractor. The cables were to be protected entirely by the angle iron, although the corners presented a problem because the bending radius of the cable bundles was sometimes limiting. The curved region below the piernose and the flat stilling basin bottom also presented a challenge, which was addressed by rolling pieces of the angle iron cable cover to a matching curvature.

Data were recorded at spillbay 4 using a Dataq DI-722 32-channel, 16-bit data acquisition instrument. Data collection was controlled by Windaq Pro+ software. Sensor analog output was digitally sampled at 2.5 kHz per channel.

At spillbay 9, data were recorded to a Sony PC216Ax 16-channel DAT recorder. Sensor output was digitally sampled at 6 kHz because the recorder automatically adjusted to 2.5 times the set frequency. Data from the DAT tapes were downloaded to computer using Sony PScanII software. Signals from dynamic and static pressure sensors at each bay were conditioned with a PCB Piezotronic Model 481 signal conditioner.

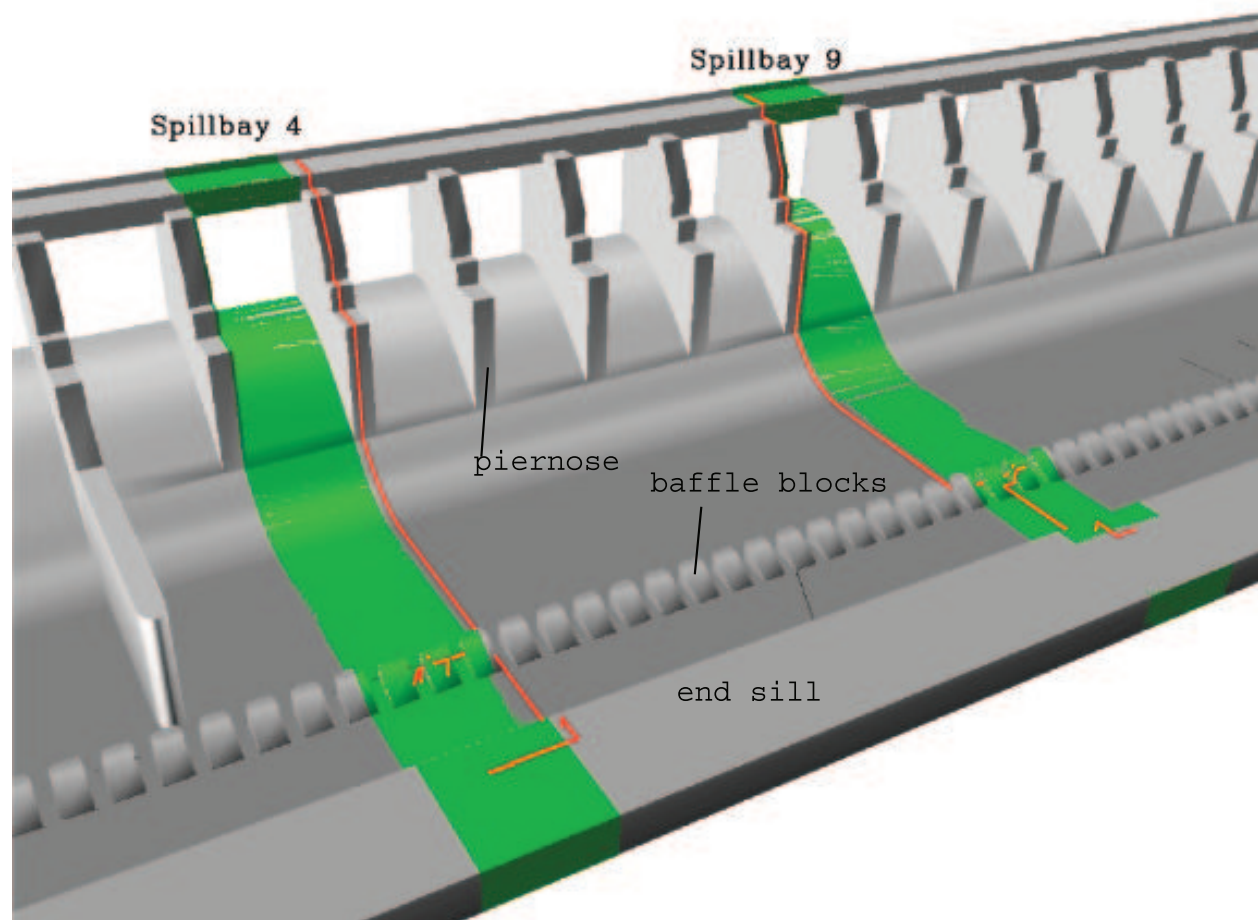


Figure 2.1: Overview of pressure transducer locations looking upstream

After spillgates were opened, flow conditions within the stilling basin were allowed to stabilize for 15 minutes for each scenario and then five minutes of pressure sensor data were recorded to tapes.

2.3 Scenarios

Data were collected for the five spill scenarios summarized in Table 2.3. The static or no spill test was done to establish a baseline and verify sensor operation. Scenario 2 involved relatively high discharge centered around spillbay 4. Scenario 5 spill was centered around spillbay 9. All spillbays between 1 and 13 were opened to discharge at moderate levels during scenario 7. The biological opinion or “biop” scenario was intended to represent the flow recommended by the biological opinion for fish passage. In this scenario, spillbays 1 - 14 were each operated, with peak discharge at spillbays 4 and 5, and decreasing discharge at the spillbays to the north and south.

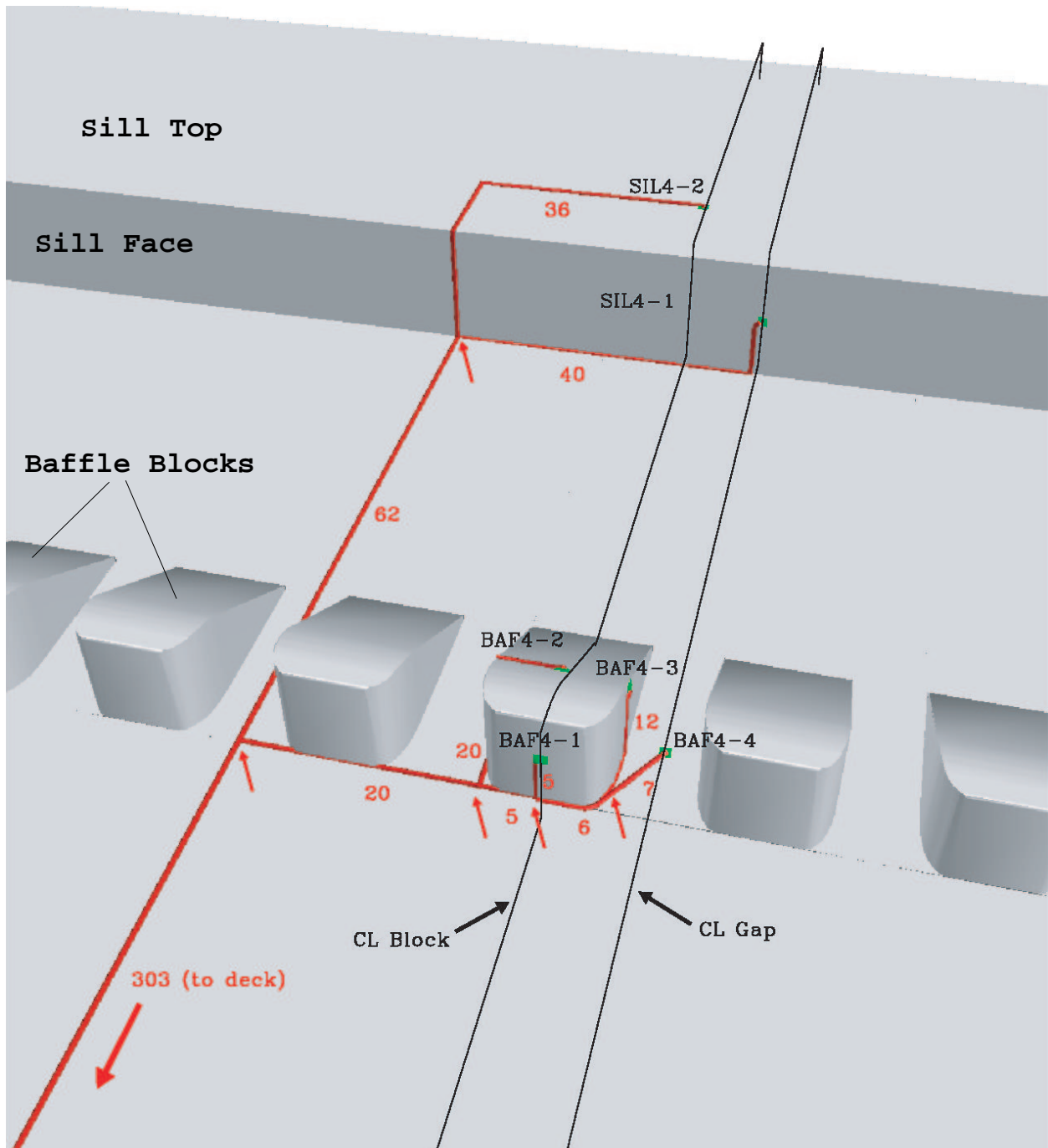


Figure 2.2: Schematic of sensor locations at spillbay 4, looking downstream (cable lengths in feet)

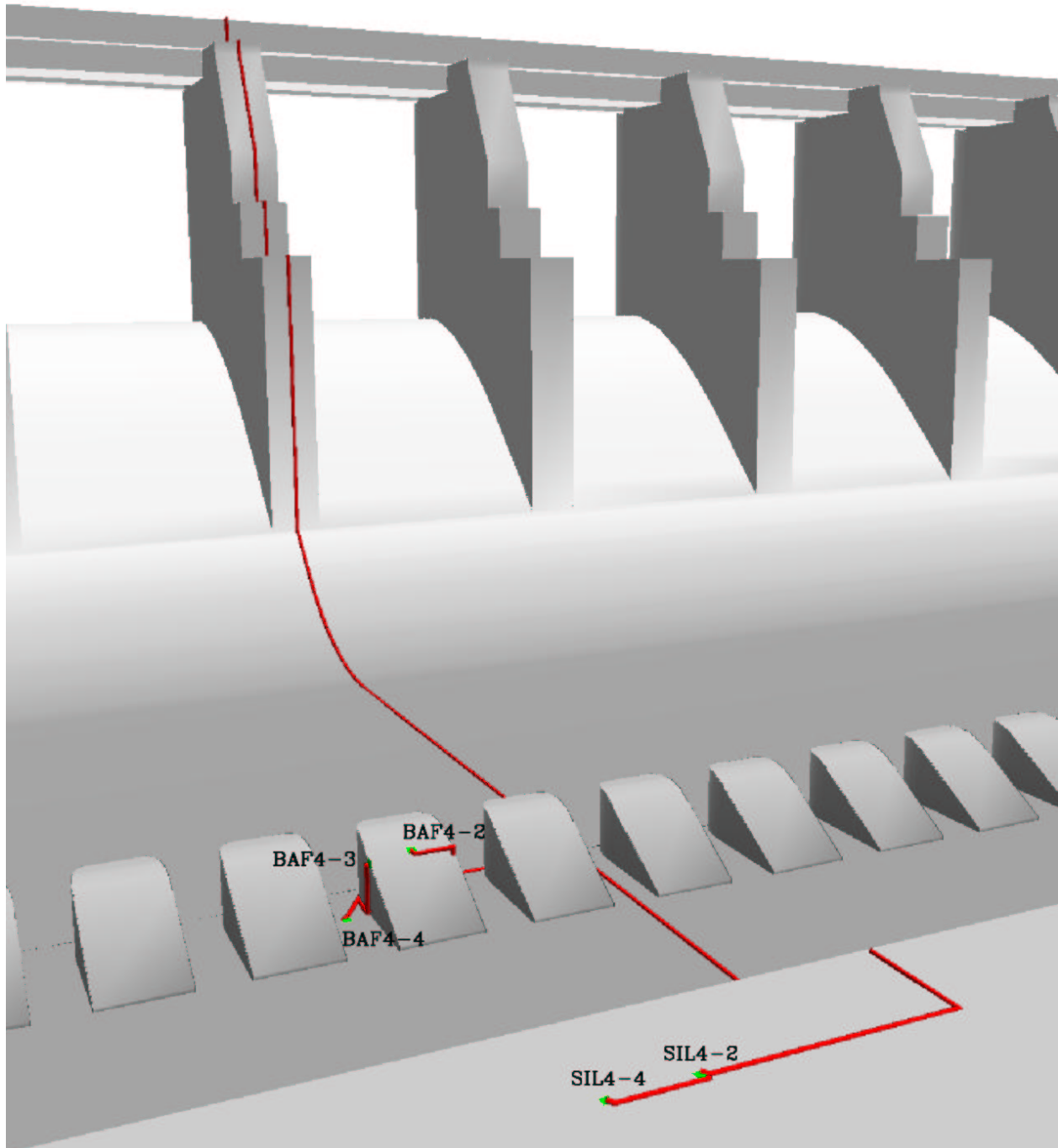


Figure 2.3: Schematic of sensor locations at spillbay 4, looking upstream

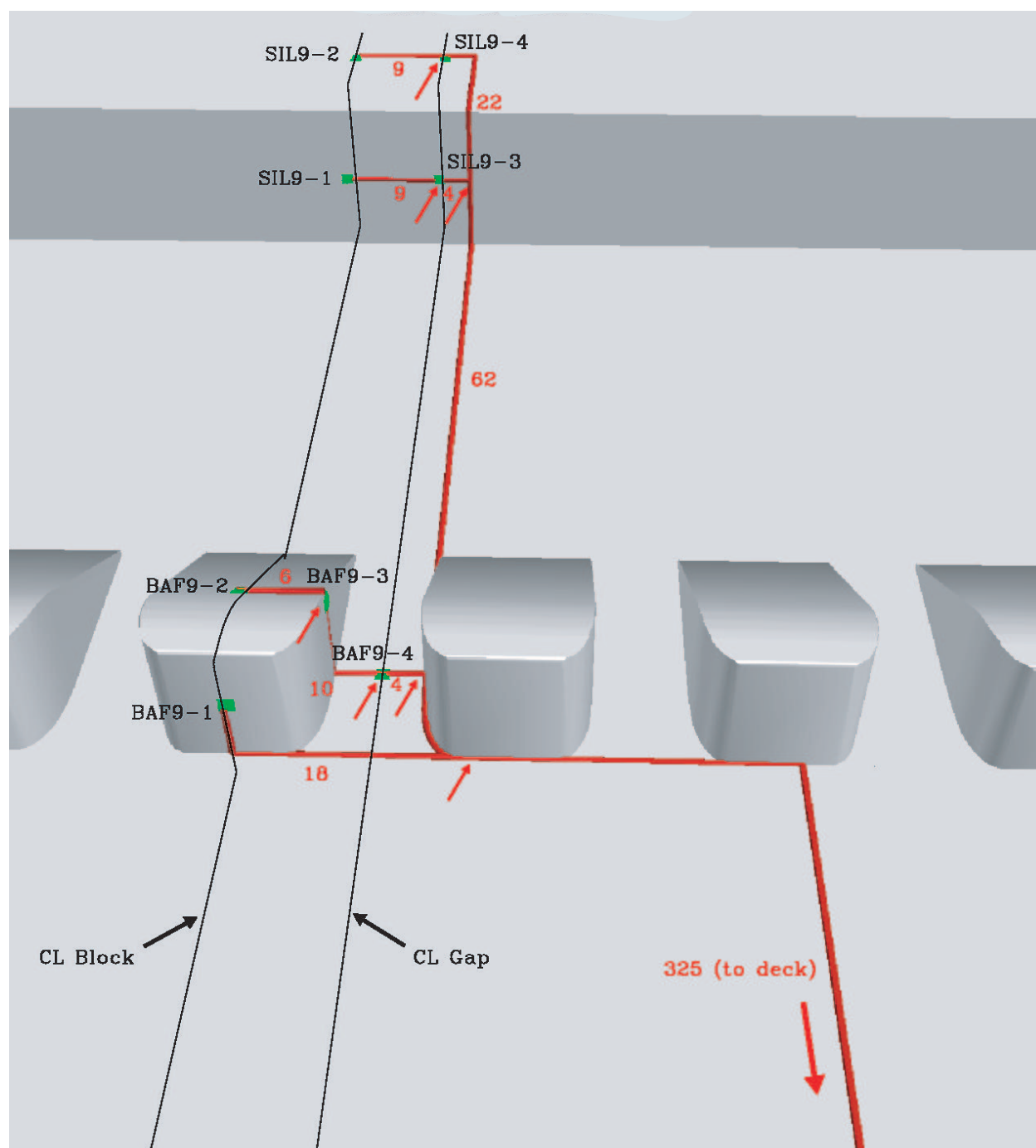


Figure 2.4: Schematic of sensor locations at spillbay 9, looking downstream (cable lengths in feet)



Figure 2.5: Sensor housings (Static sensor is in housing with triangular cover)



Figure 2.6: Dynamic sensor housing showing flush-mounted front face and protective sensor cover protruding from the back



Figure 2.7: Angle iron and flange used to cover cable runs, and coiled cable bundles covered with vacuum tubing

2.4 Analysis

The data that were used for the statistics, power spectra, and probability density functions were all analyzed using DADiSP, a graphical data analysis and visualization software package. In DADiSP, the data were converted from volts to pounds per square inch (psi), and normalized by subtracting the mean and dividing by the standard deviation.

The spillbay 4 data were imported at 2500 samples/s and the spillbay 9 data were imported at 3000 samples/s. The data for spillbay 9 were originally collected at 6000 samples/second, but were decimated upon import into DADiSP. Five minute samples were taken for most sensors; however, some of the channels had shorter sample times due to sensor failure.

FLOW3D, a three-dimensional CFD model, was used to simulate the flow in a Dalles Dam spillbay and the corresponding downstream region within the stilling basin at scenario 2 and scenario 5 conditions. Output nodes were inserted in locations equivalent to where the pressure sensors were located in the field. The pressure data output from the CFD model were then processed in the same manner as the empirical pressure data and corresponding simulated and measured data were compared.

2.4.1 Summary Statistics

DADiSP was used to calculate the mean and standard deviation for each channel and scenario. The summary statistics were imported into Microsoft Excel, where the pressure units were converted from psi to feet of water.

2.4.2 Power Spectra

DADiSP was used to process the data and generate power spectrum plots for each sensor and scenario. The data for each channel from each scenario were normalized to have a mean of zero and a standard deviation of 1. Then they were sectioned or binned into 20 equal sections. The data were not filtered. A power spectrum was generated for each bin. Finally, the power spectra for all the bins or sections were averaged to create the final mean power spectrum for the scenario. This technique was used to decrease the presence of 60 cycle noise that was obtained from the power source at The Dalles Dam. The power spectra shows the energy per unit time within the frequency band selected for analysis. Frequencies with higher energy show as peaks in the mean power spectra.

The normalized static sensor data were also subtracted from the dynamic sensor data in an attempt to isolate the higher frequency turbulence and eliminate effects due to wave action. However, subtracting the static data seemed to make no difference in the resulting power spectrum, so this analytical approach was not pursued further.

2.4.3 Probability Density Functions

A histogram was created in DADiSP for the pressure data from each sensor at each scenario to determine the characteristics of the dataset distribution. The vertical axis was converted to a ratio of the number of counts to the total number of counts. A normal curve was created for the histogram using the equation $y = \frac{1}{\sigma\sqrt{2\pi}} e^{-\frac{(Xi-\mu)^2}{2\sigma^2}}$, where Xi is the pressure data value, μ is the mean and σ is the standard deviation. The normal curves were overlotted on the histogram.

Table 2.3: Flow scenarios in kcfs

Spillbay	Static	Scenario 2	Scenario 5	Scenario 7	Biop
1	0	1.5	-	3.0	3.0
2	0	3.0	-	3.0	4.0
3	0	6.0	-	4.5	4.0
4	0	6.0	-	4.5	5.0
5	0	6.0	-	4.5	5.0
6	0	3.0	1.5	4.5	4.0
7	0	1.5	3.0	4.5	4.0
8	0	-	6.0	4.5	3.0
9	0	-	6.0	4.5	3.0
10	0	-	6.0	4.5	3.0
11	0	-	3.0	3.0	3.0
12	0	-	1.5	3.0	3.0
13	0	-	-	3.0	2.0
14	0	-	-	-	2.0
15	0	-	-	-	-
16	0	-	-	-	-
17	0	-	-	-	-
18	0	-	-	-	-
19	0	-	-	-	-
20	0	-	-	-	-
21	0	-	-	-	-
22	0	-	-	-	-
23	0	-	-	-	-

3 Results

3.1 Sensor Survival

Initially, 12 sensors were mounted in spillbay 4. The sensors were labeled according to their tape recorder channel (channels 1 through 12) and also by their location and type (e.g., baffle dynamic 1). Table 3.1 provides a summary of sensor survival in spillbay 4. Sensors 11 and 12 failed immediately. The remaining sensors, 1 through 10, were all operational for the static scenario. Sensors 6, 10, and 12 were pulled during the flow rampup for scenario 2. Sensors 5 and 9 failed during scenario 2, although data were collected for the time they were working. Sensors 1 through 4, 7, and 8 operated normally for scenario 5 and scenario 7. Sensor 8 failed during the biop flow scenario, but data were collected for the time it was working.

Sensors 1 through 16 were installed in Spillbay 9, except for sensor 7, which was never installed. Table 3.2 provides a summary of sensor survival in spillbay 9. All the sensors worked for the static scenario and scenario 2. Sensors 1 through 4, 8,9, and 11 failed during the setup for scenario 5. Sensors 5, 12, 13, and 15 failed during scenario 5. However, data were still retrieved from sensors 5, 13, and 15 for a portion of the scenario. The remaining sensors, 6, 10, 14, and 16, remained operational during scenario 7 and the biop scenario.

3.2 Sensor Statistics

The trends in the summary statistics of the pressure data during the different scenarios conform in many cases to the flow patterns that would be expected around the tailrace structures (e.g., high-velocity flow forcefully hitting the upstream face of the baffle blocks and endsill, and flow separation occurring on top of the structures) (Tables 3.3 and 3.4). The mean pressure for each sensor was comparable to the depths of the sensors during the static tests. The static sensor for the face of either the sill or baffle block showed an increase in pressure when subjected to direct flow. The static sensors on top of the structures generally showed a decrease in pressure under head-on flow. Nearly all sensors exhibited an increase in variability when subjected to higher discharges. The dynamic sensors measured instantaneous relative pressure change and therefore had means near zero did not exhibit the aforementioned trends.

3.3 Power Spectra

The following process was used to generate the power spectra. The raw data were normalized by subtracting the mean from each data point and dividing by the standard deviation. The normalized data were then binned into 20 equal sections and a power spectra was generated for each bin. The power spectra samples were then averaged to generate the mean power spectrum for the dataset. The power spectra plots show the signal strength with respect to frequency for the component waveforms of the data. Plots for all the data are shown in the appendices.

3.3.1 Power Spectra Comparisons

Data from Spillbay 4 were overplotted in various combinations to emphasize notable trends. Since all spillbay 9 sensors failed during the first exposure to high flows in scenario 5, only data from spillbay 4 are discussed here. Plots of all the usable data from each spillbay are included in the appendix. The static sensor on the sill face at spillbay 4 showed an increase in mean pressure and low-frequency spectral power, and a decrease in high-frequency spectral power when subjected to head-on flow (Figure 3.1). A peak was also evident at 90 Hz for scenario 2 but not for the static (ambient) test.

Table 3.1: Spillbay 4 sensor survival

Chnl	Location	Type	Static	Scenario 2	Scenario 5	Scenario 7	Biop
1	Sill Top	Dynamic	ok	ok	ok	ok	ok
2	Sill Top	Static	ok	ok	ok	ok	ok
3	Sill Face	Dynamic	ok	ok	ok	ok	ok
4	Sill Face	Static	ok	ok	ok	ok	ok
5	Baffle Face	Dynamic	ok	failed	—	—	—
6	Baffle Face	Static	ok	—	—	—	—
7	Baffle Top	Dynamic	ok	ok	ok	ok	failed
8	Baffle Top	Static	ok	ok	ok	ok	failed
9	Baffle Side	Dynamic	ok	failed	—	—	—
10	Baffle Side	Static	ok	—	—	—	—
11	Baffle Chnl	Dynamic	—	—	—	—	—
12	Baffle Chnl	Static	—	—	—	—	—

Table 3.2: Spillbay 9 sensor survival

Chnl	Location	Type	Static	Scenario 2	Scenario 5	Scenario 7	Biop
1	Baffle Face	Dynamic	ok	ok	—	—	—
2	Baffle Face	Static	ok	ok	—	—	—
3	Baffle Top	Dynamic	ok	ok	—	—	—
4	Baffle Top	Static	ok	ok	—	—	—
5	Baffle Side	Dynamic	ok	ok	—	—	—
6	Baffle Side	Static	ok	ok	failed	—	—
7	Baffle Floor	Dynamic	—	—	—	—	—
8	Baffle Floor	Static	ok	ok	—	—	—
9	Sill Face	Dynamic	ok	ok	—	—	—
10	Sill Face	Static	ok	ok	failed	—	—
11	Sill Top	Dynamic	ok	ok	—	—	—
12	Sill Top	Static	ok	ok	—	—	—
13	Sill Face	Dynamic	ok	ok	—	—	—
14	Sill Face	Static	ok	ok	failed	—	—
15	Sill Top	Dynamic	ok	ok	—	—	—
16	Sill Top	Static	ok	ok	failed	—	—

Table 3.3: Spillbay 4 sensor mean (μ) and standard deviation (σ) in ft of water for all tests (note, dynamic sensor means are near zero, and the static sensor means are similar to the sensor depth, with the exception of channel 6, which was probably malfunctioning already during the static test)

Chnl	Loc	Type	Depth (ft)	Static	Sc 2	Sc 5	Sc 7	Biop
				$\mu(\sigma(ft))$	$\mu(\sigma(ft))$	$\mu(\sigma(ft))$	$\mu(\sigma(ft))$	$\mu(\sigma(ft))$
1	Sill Top	Dyn	11.5	0.106 (0.119)	0.123 (0.582)	0.178 (0.172)	0.146 (0.307)	0.177 (0.589)
3	Sill Face	Dyn	17.5	0.132 (0.081)	0.1645(0.600)	0.211 (0.103)	0.170 (0.307)	0.213 (0.605)
5	Baffle Face	Dyn	20.5	0.003 (0.052)	0.003 (0.052)			
7	Baffle Top	Dyn	17.2	0.117 (0.137)	0.165 (0.155)	0.200 (0.102)	0.164 (0.088)	0.202 (0.088)
9	Baffle Side	Dyn	20.5	0.000 (0.054)	-0.001 (0.528)			
2	Sill Top	Stat	11.5	10.579 (0.131)	9.311 (1.052)	9.261 (0.221)	11.037 (0.511)	10.009 (1.014)
4	Sill Face	Stat	17.5	15.351 (0.123)	18.763 (0.962)	14.027 (0.180)	16.842 (0.631)	18.645 (1.165)
6	Baffle Face	Stat	20.5	33.076 (1.359)				
8	Baffle Top	Stat	17.2	15.475 (0.125)	12.093 (1.876)	14.026 (0.190)	15.227 (1.514)	9.563 (1.243)
10	Baffle Side	Stat	20.5	21.470 (0.120)				

Table 3.4: Spillbay 9 sensor mean (μ) and standard deviation (σ) in ft of water for all tests. Note, dynamic sensor means are near zero, and the static sensors means are similar to the sensor depth

Chnl	Loc	Type	Depth (ft)	Static	Sc 2	Sc 5	Sc 7	Biop
				$\mu(\sigma(ft))$	$\mu(\sigma(ft))$	$\mu(\sigma(ft))$	$\mu(\sigma(ft))$	$\mu(\sigma(ft))$
1	Baffle Face	Dynamic	20.5	0.033 (0.085)	-0.004 (0.083)			
3	Baffle Top	Dynamic	17.2	0.026 (0.063)	0.015 (0.091)			
5	Baffle Side	Dynamic	20.5	0.032 (0.066)	0.019 (0.091)	-0.066 (0.982)		
9	Sill Face	Dynamic	17.5	0.021 (0.037)	0.009 (0.085)			
11	Sill Top	Dynamic	11.5	0.019 (0.077)	0.009 (0.169)			
13	Sill Face	Dynamic	17.5	0.027 (0.043)	0.021 (0.082)	0.022 (0.069)		
15	Sill Top	Dynamic	11.5	0.025 (0.082)	0.021 (0.081)	6.883 (0.660)		
2	Baffle Face	Static	20.5	17.222 (0.028)	16.842 (0.102)			
4	Baffle Top	Static	17.2	15.884 (0.026)	15.484 (0.105)			
6	Baffle Side	Static	20.5	21.933 (0.030)	21.521 (0.099)	16.335 (2.322)		
8	Baffle Floor	Static	24.5	23.602 (0.027)	23.210 (0.100)			
10	Sill Face	Static	17.5	15.109 (0.028)	14.682 (0.118)	19.618 (1.137)		
12	Sill Top	Static	11.5	10.720 (0.030)	10.334 (0.197)			
14	Sill Face	Static	17.5	15.414 (0.028)	14.999 (0.114)	19.474 (1.001)		
16	Sill Top	Static	11.5	10.600 (0.026)	10.179 (0.189)	9.786 (1.084)		

The static sensor on top of the endsill showed an overall decrease in mean pressure and a substantial increase in low-frequency spectral power during heavy oncoming flow as compared to ambient conditions (Figure 3.2). A peak in the scenario 2 data also existed at a frequency of approximately 150 Hz.

At the endsill face, the dynamic sensor had a mean of zero and a similar spectra to the static sensor with a small peak at 2 Hz (Figure 3.3). The dynamic sensor lacked the peak at 90 Hz, however.

The signals from the static sensors mounted on the top and face of the endsill below spillbay 4 were similar (Figure 3.4). The overall mean pressure at the sill face was higher, however, because that sensor was mounted deeper in the water column. The power spectra of the data had relatively high-frequency peaks of approximately 90 and 150 Hz for the face and top sensors, respectively. The data from the sensor on the face of the endsill also showed a small peak around 2 Hz, which could represent a hydraulic phenomenon.

The signals from the static sensors mounted on the top of the endsill and the top of the baffle block below spillbay 4 were similar as well (Figure 3.5). The sensor on the baffle top was mounted slightly deeper in the water and in a more turbulent region with higher amplitude, lower frequency fluctuations. The power spectra of the data had peaks with relatively high frequencies of approximately 100 and 150 Hz for the baffle block and endsill sensors, respectively.

3.3.2 Comparison with CFD Results

The data from the static sensor mounted to the face of the endsill below spillbay 4 was similar in magnitude to the simulated hydraulic data (Figure 3.6). The measured signal was substantially more variable, however, which was evidenced by the fact that the power spectra for the measured data were offset to higher frequencies by approximately half an order of magnitude. Trends similar to these were also observed between simulated and measured data for the top of the spillbay 4 endsill (Figure 3.7) and the top of the baffle block at spillbay 4 (Figure 3.8). Although, the magnitude of the simulated pressures was slightly higher than the measured data at the top of the spillbay 4 baffle block. The power spectra of the simulated data were cut off at 50 Hz because that is the highest frequency that can be resolved given the 0.01 sec model time.

3.4 Probability Density Functions

Probability density functions of the pressure data were generated and plotted with normal curves computed from the mean and standard deviation of each sample. The skewness and kurtosis of the datasets, shown in Table 3.5, were also calculated to estimate deviation from normality of the datasets more quantitatively. In general, the datasets were not normally distributed, although they were close in some cases. Pressure data collected during ambient flow conditions were very peaked and positively skewed (top and middle left in Figure 3.9). Data collected on the sill face during scenario 2 were less skewed, although still steeper than the normal curve, and had a broad tail of very low occurrence high pressure data (top and 2nd from top right in Figure 3.9). This suggests that low frequency, high pressure events may occur on the face. Alternatively, the sill and baffle top data have slight tails in the negative direction (lower left, lower right and 2nd from bottom right Figure 3.9), suggesting that pressure reducing events are common on the top. These observations

indicate that it may be difficult to estimate the probability of high pressure events using standard parametric measures of central tendency and variability.

Table 3.5: Depth, mean (μ), standard deviation (σ), skewness, and kurtosis values for datasets included in this report. The skewness and kurtosis parameters reflect the normality of the data.

Chnl	Loc	Type	Scenario	Depth (ft)	$\mu(ft)$	$\sigma(ft)$	skewness (g)	kurtosis
2	Sill Top	Stat	Ambient	11.5	10.579	0.131	3.566	96.965
3	Sill Face	Dyn	Scenario 2	17.5	0.1645	0.600	0.665	1.797
4	Sill Face	Stat	Ambient	17.5	15.351	0.123	4.799	167.522
4	Sill Face	Stat	Scenario 2	17.5	18.763	0.962	0.717	2.189
2	Sill Top	Stat	Scenario 2	11.5	9.311	1.052	-0.270	1.601
7	Baffle Top	Dyn	Scenario 2	17.2	0.165	0.155	0.016	5.669
8	Baffle Top	Stat	Scenario 2	17.2	12.093	1.876	-0.511	1.932

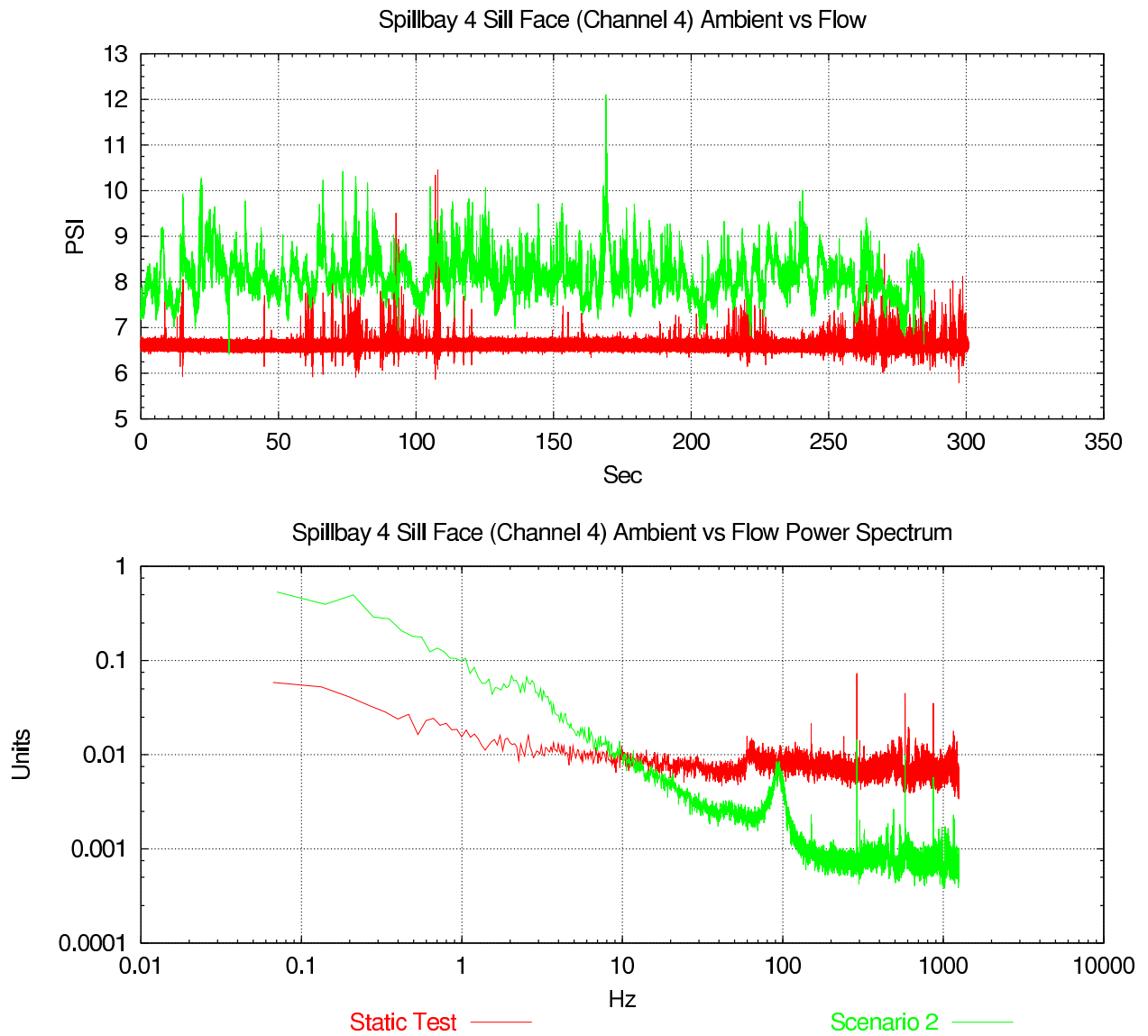


Figure 3.1: Comparison of ambient or static conditions versus scenario 2 results at the static sensor on the spillbay 4 sill face

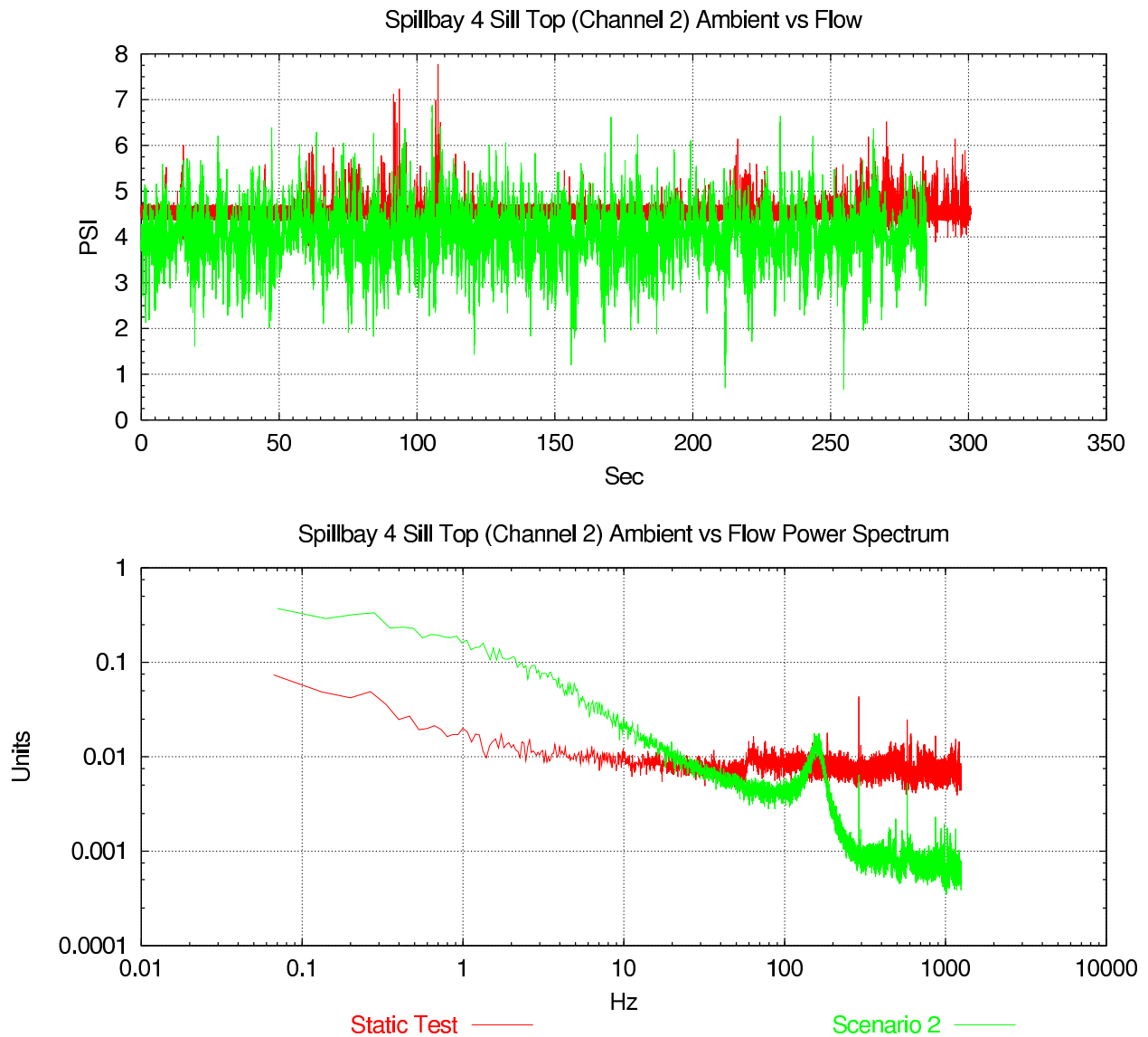


Figure 3.2: Comparison of static or ambient conditions and scenario 2 results for the static sensor on top of the spillbay 4 endsill

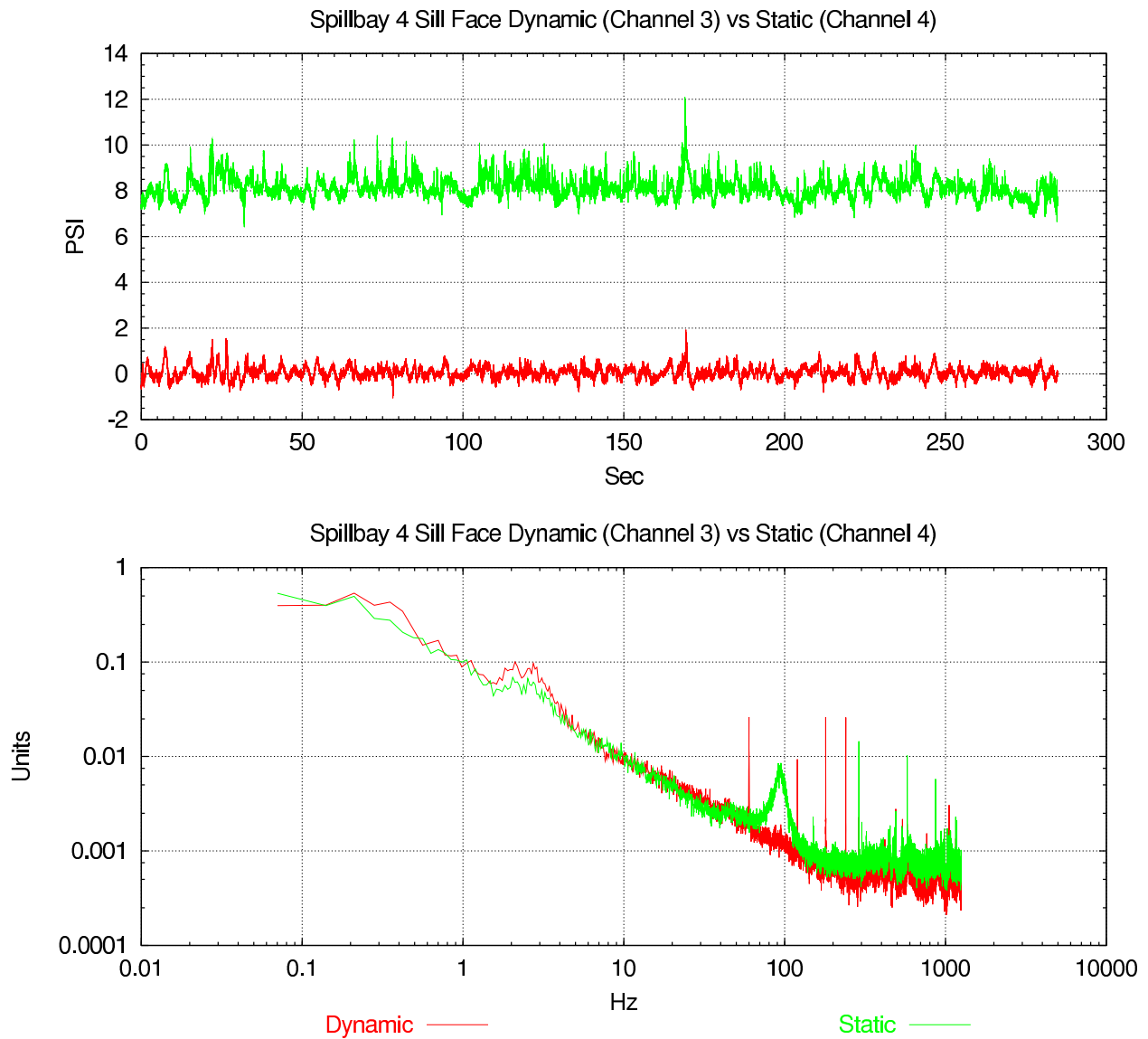


Figure 3.3: Comparison of static versus dynamic results for the sensors on the face of the endsill below spillbay 4 during scenario 2

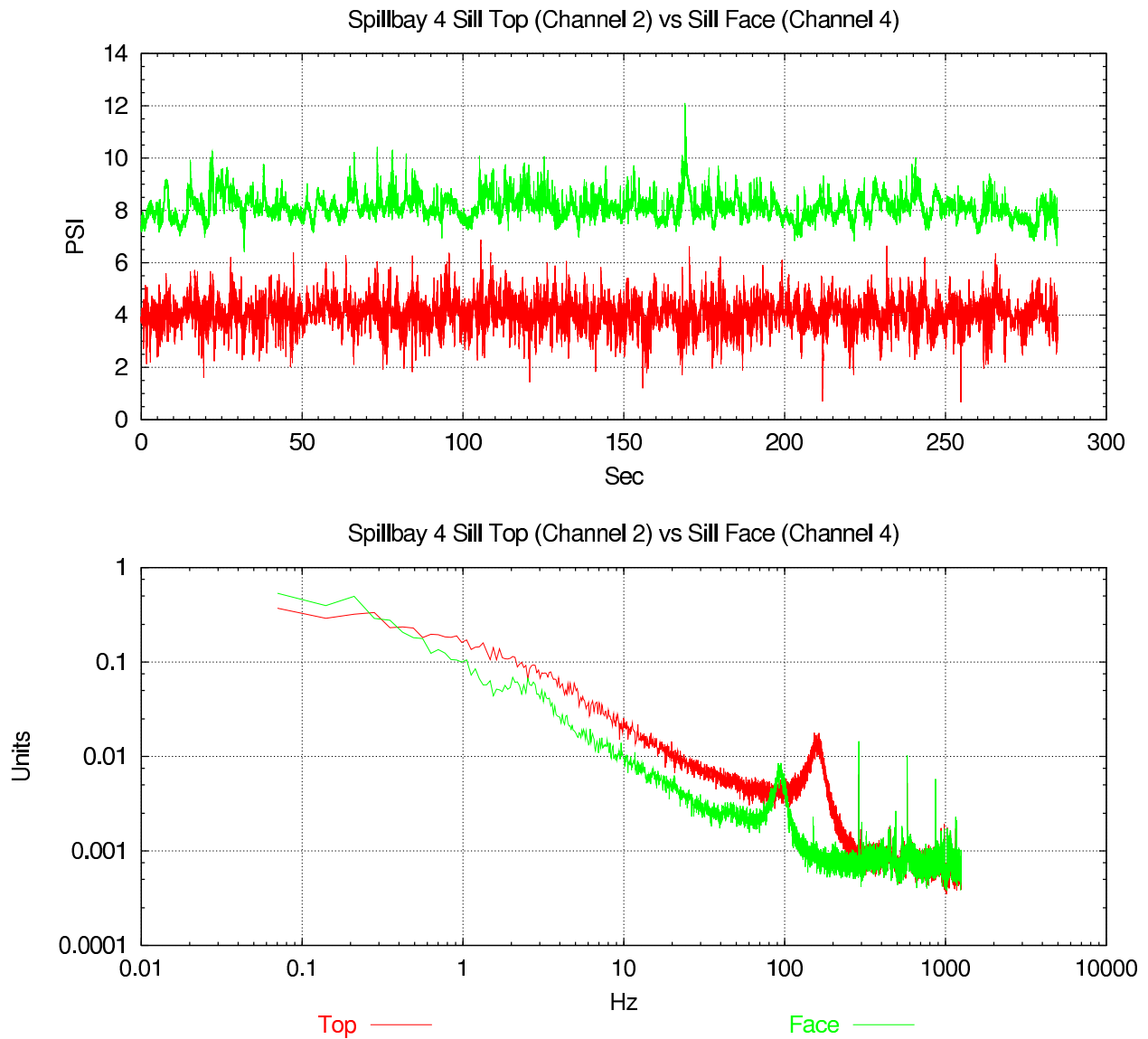


Figure 3.4: Comparison of top versus face results for the static sensors on the endsill below spillbay 4 during scenario 2

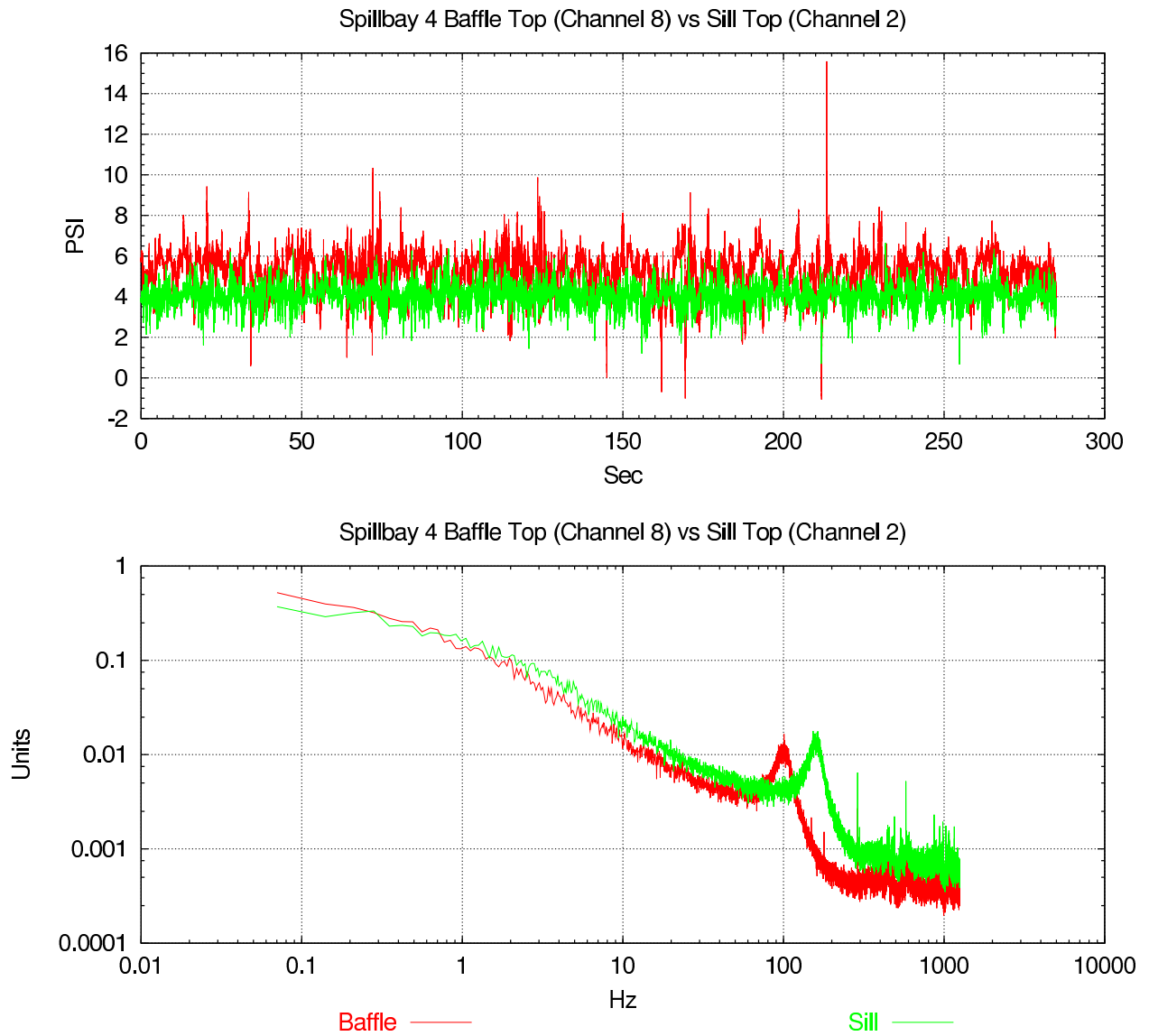


Figure 3.5: Comparison of results for the sill top and baffle top static sensors at spillbay 4 during scenario 2

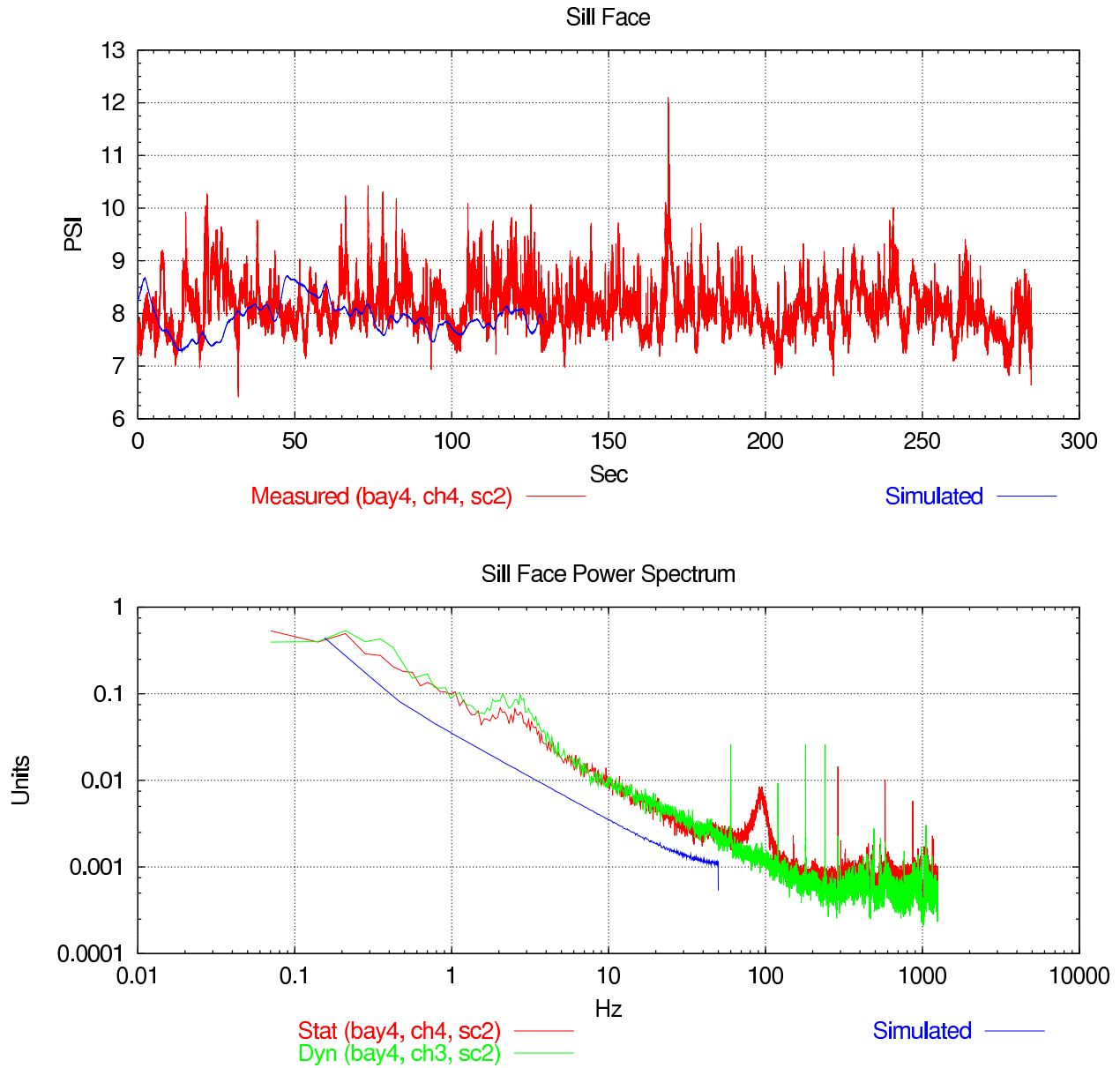


Figure 3.6: Comparison of simulated and measured data on the face of the spillbay 4 endsill for scenario 2 conditions

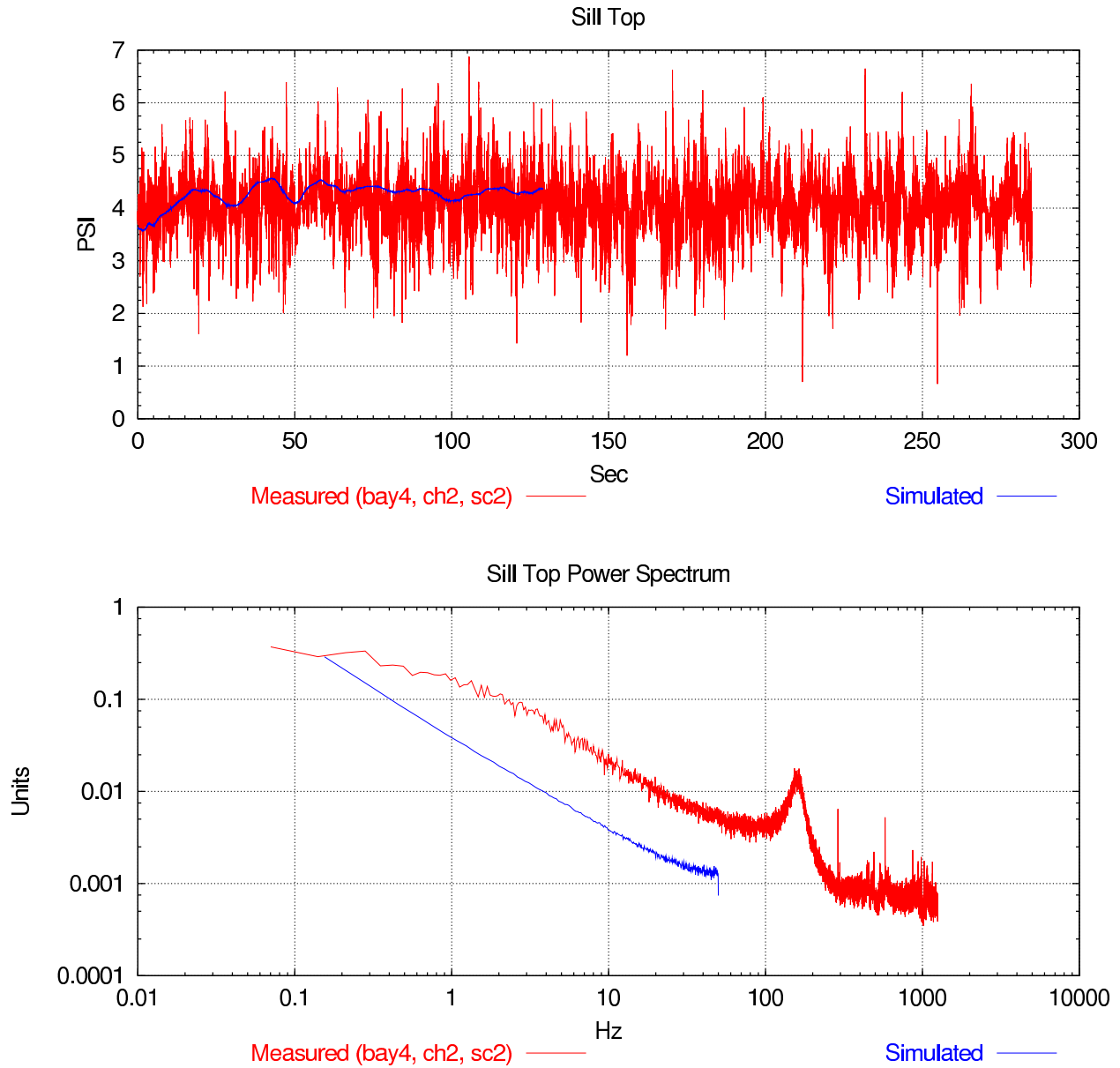


Figure 3.7: Comparison of simulated and measured results at the top of the spillbay 4 endsill for scenario 2 conditions

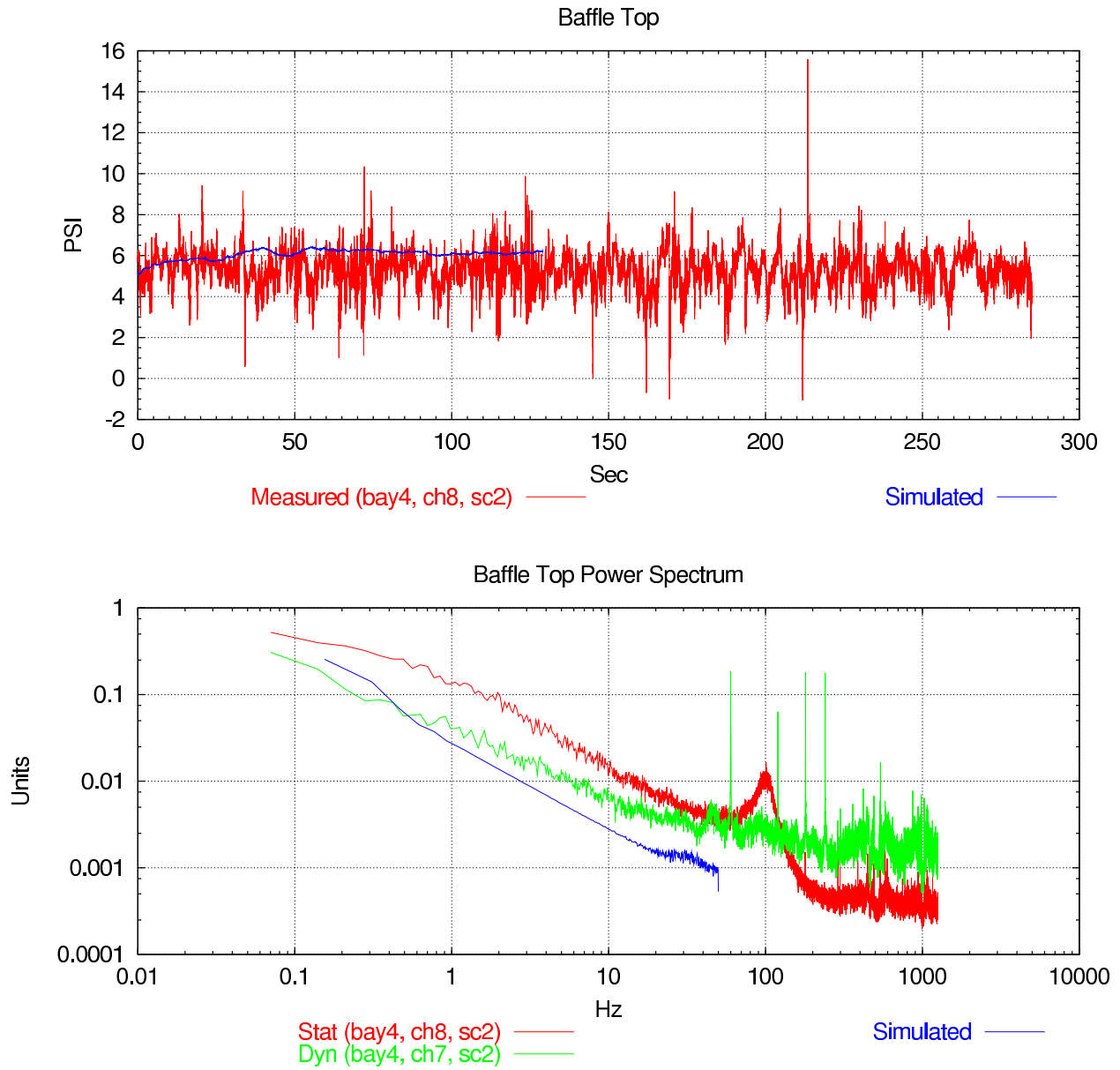


Figure 3.8: Comparison of simulated and measured results at the top of the spillbay 4 baffle block for scenario 2 conditions

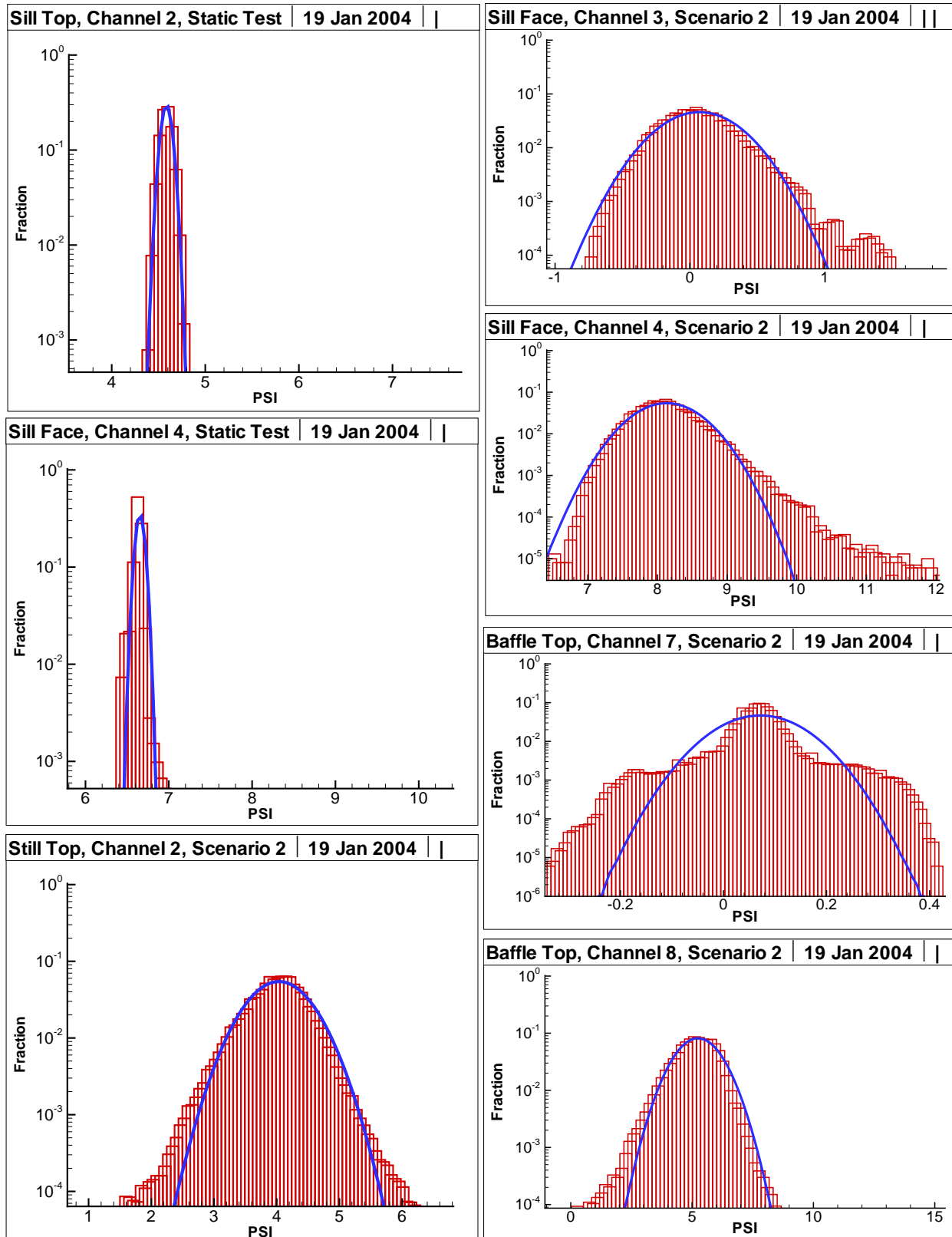


Figure 3.9: Spillbay 4, probability density plots for selected sensors and scenarios

4 Discussion

The hydraulic environment in The Dalles stilling basin during high or even moderate spillway discharge is extremely turbulent. Figure 4.1 shows the region at the base of the spillway 4 ogee, and Figure 4.2 shows the region over the baffles and endsill. Notice the large standing wave just downstream of the endsill. Mounting relatively delicate instruments requiring cable connections in such an environment is a difficult task. The difficulty is further compounded when the mounting must be done underwater.

Inspection of the equipment following the tests indicated that the failures occurred in the main trunkline and in a number of places in the branches further downstream. The main trunkline failed in the curved region between the bottom of the piernose and the flat bottom of the stilling basin (see Figure 2.1). This may have occurred because the curvature of the angle iron cable covers did not conform sufficiently to the curvature of the bottom, either in radius of curvature or arc length. The angle iron cable covers also pulled out at the base of the endsill in many places. This failure is somewhat surprising because the base of the endsill was expected to be a relatively low-velocity



Figure 4.1: Spillbay 4 at high discharge



Figure 4.2: Flow above baffle and endsill downstream of spillbay 4 (note the large standing wave just downstream of the endsill)

region. The sensors themselves appear to have remained intact in many cases. In the future, cable routings should be designed to avoid these failure regions and made substantially more robust with more frequent and deeper bolts.

The amount of noise in the pressure signal presented challenges during data processing. Band pass and band block filtering techniques were not effective and changed the spectral nature of the data. Applying a running average helped reduce noise, but eliminated most peaks in the process. Subtracting the demeaned static data from the corresponding dynamic data for a given sensor pair did little to change the power spectrum of the dynamic sensor data and did not seem to have the anticipated effect of removing the low-frequency wave signals and isolating the turbulence-related high-frequency phenomena. Ultimately, the most effective approach was to bin the data into 20 equally sized sections, compute power spectra for each section, and then calculate an overall average.

The summary statistics of the data followed several expected trends. The mean pressures were proportional to depth and incident flow velocity, variability increased with oncoming flow, and data from sensors on top of structures decreased in pressure in flow separation zones. Using the relationships posed by Toso and Bowers (1988) and Bowers and Tsai (1969), the standard deviation

can be used to estimate the incident velocity to the baffle and endsill. The authors each concluded that total pressure fluctuations about the mean in a hydraulic jump are on the order of 80% of the incident velocity head and that they can be 10-20 times the rms of the pressure. This relationship can be expressed as

$$0.8 * \frac{v^2}{2g} = 10 * rms.$$

Using this relationship and substituting the standard deviation (σ) of the pressure for the rms, we estimated the incident velocity to the endsill as

$$v = \sqrt{\frac{2g10\sigma}{0.8}} = \sqrt{\frac{2 * 32.2 * 10 * 0.96}{0.8}} = 27 ft/s.$$

This corresponds to the 17-22 ft/s velocity range predicted by the CFD model results for the endsill and baffle block below spillbay 4 during scenario 2.

The spectral plots of the data showed only a few spikes at low enough frequencies to result from large-scale wave action, turbulent bursting, or localized turbulence. Some low-frequency bumps or spikes existed below 10 Hz in the endsill data, which may have resulted from wave action or turbulent flow. The other prominent peaks observed were in the high-frequency range of the data (90 - 150 Hz) for only the static sensors. These peaks were probably due to either electrical noise, micro-scale vortex shedding off the static sensor housing, or sensor failure in some cases. The fact that these high-frequency signals were observed for only the static sensor data suggests that they resulted from vortex shedding off of the static sensor housings, which were not flush to the bottom surface like the dynamic sensors housings were.

Pressure data generated by the CFD model, when compared to the measured data, was sometimes slightly lower in magnitude, had a similar slope in the power spectrum, and generally had a lower frequency response. The mean pressures reported by the CFD model probably differed because the true depth of the sensors below the water surface at each scenario was not known exactly. The primary reason for the lower frequency response is that the CFD model represents turbulence using the Reynolds-averaged Navier-Stokes equations together with a two-equation RNG turbulence model. This type of model, while unsteady, does not capture high-frequency pressure and velocity fluctuations. Additionally, the model timestep was 0.01 s, which is much lower than the frequency of the pressure measurements. Finally, the model was run under steady state boundary conditions, which eliminates the velocity fluctuations that may result from variations in headwater and tailwater elevations.

5 Conclusions and Recommendations

An effective data processing approach for high-frequency pressure data was to bin the data into 20 equally sized sections, compute power spectra for each section, and then average them all together. The magnitude and variability of the static sensor data generally corresponded with water depth and oncoming velocity. In addition, the endsill pressure data showed spectral peaks below 10 Hz that may be of hydraulic origin and at spatial and temporal scales that have an impact on fish. Based on the mean and standard deviation of the static sensor data, the incident velocity to the endsill face could be between 15 and 25 ft/s and could fluctuate 11 ft/s about the mean. These incident velocity estimates correspond well with estimates obtained from CFD model data. Power spectra of pressure data generated with the CFD model had similar spectrum shape to measured data, but frequencies of the modeled data were 0.5 to 1 order of magnitude lower. This discrepancy is due primarily to the properties of the Reynolds-averaged Navier-Stokes equations used in the CFD model.

In the future, cable routings for instrumentation installed in a stilling basin environment should be designed to avoid the failure regions observed here, especially the curved region of the ogee. Routings should also be made substantially more robust with more frequent and deeper studs. Sensors should be mounted flush to the surface with no housing protruding so that additional vortex-shedding does not occur near the pressure transducer head to create unnecessary noise and complicate the interpretation of the data.

6 References

- Armenio, V., P. Toscano, and V. Fiorotto. 2000. On the effects of a negative step in pressure fluctuations at the bottom of a hydraulic jump. *J. Hydr. Res.*, 38(5): 359-368.
- Bowers, C.E., and F.Y. Tsai. 1969. Fluctuating pressures in spillway stilling basins. *J. Hydr. Div. Proc ASCE*, 95(HY6): 2071-2079.
- Bull, M.K. 1996. Wall pressure fluctuations beneath turbulent boundary layers: Some reflections on forty years of research. *J. Sound Vibr.*, 190(3): 299-315.
- Elgar, S., T.H.C. Herbers, V. Chandrin, and R.T. Guza. 1995. Higher-order spectral analysis of nonlinear ocean surface gravity waves. *J. Geophys. Res.*, 100(C3): 4977-4983.
- Herbers, T.H.C. and R.T. Guza. 1994. Nonlinear wave interactions and high-frequency seafloor pressure, *J. Geophys. Res.*, 99(C5): 10,035-10,048.
- Keir, G., T.E. Unny, and H.M. Hill. 1969. Pressure fluctuations on submerged sluice gate. *J. Hydr. Div. ASCE* 95(HY6): 1781-1791.
- Lauchle, G.E., and W.A. Kargus IV. 2000. Scaling of turbulent wall pressure fluctuations downstream of a rearward facing step. *J. Acoust. Soc. Am.* 107(1): L1-L6.
- Toso, J.W., and C.E. Bowers. 1988. Extreme pressures in hydraulic-jump stilling basins. *J. Hydr. Eng.* 114(8): 829-843.

A Spillbay Raw Data and Power Spectra

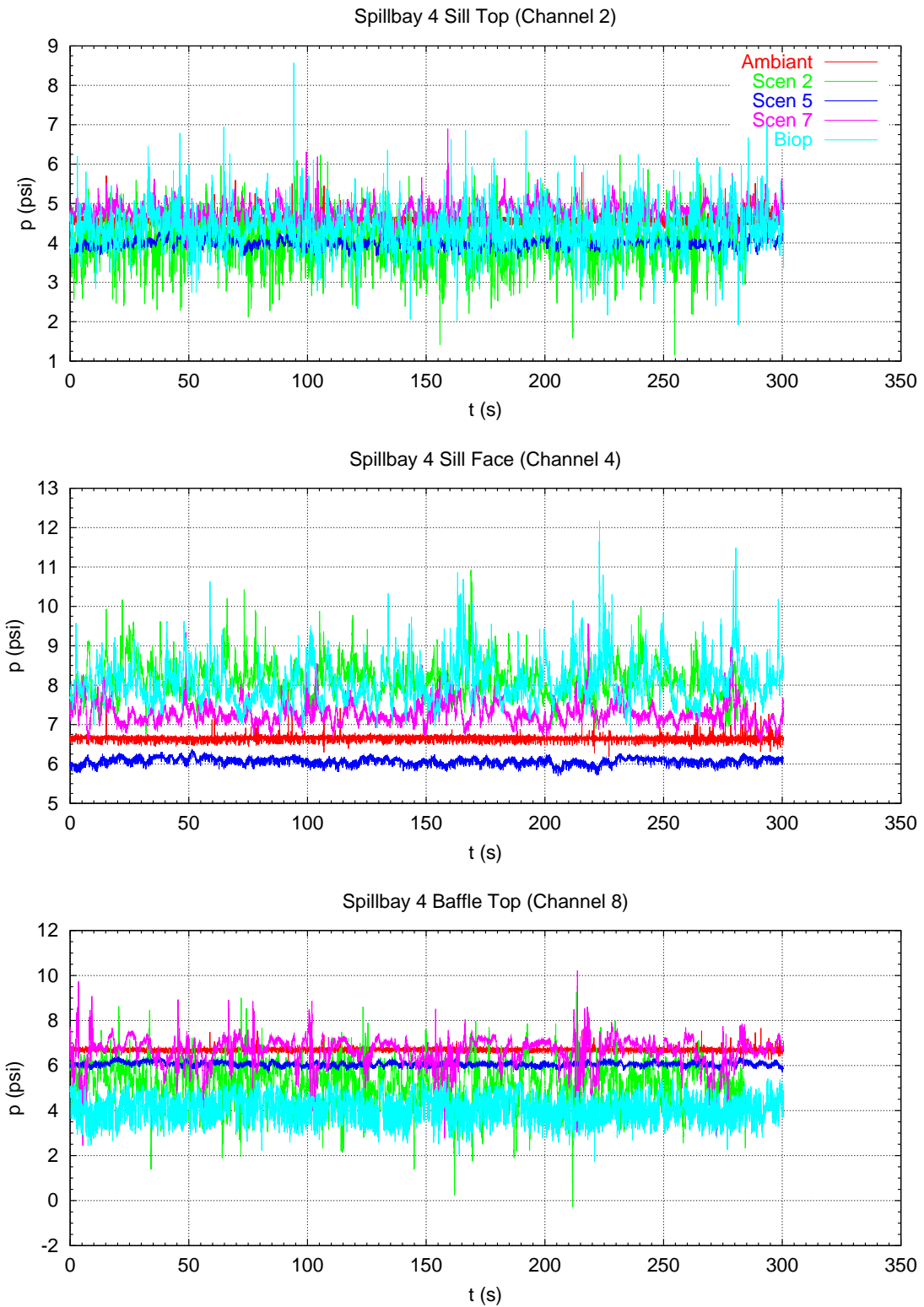


Figure A.1: Static sensor data from spillbay 4

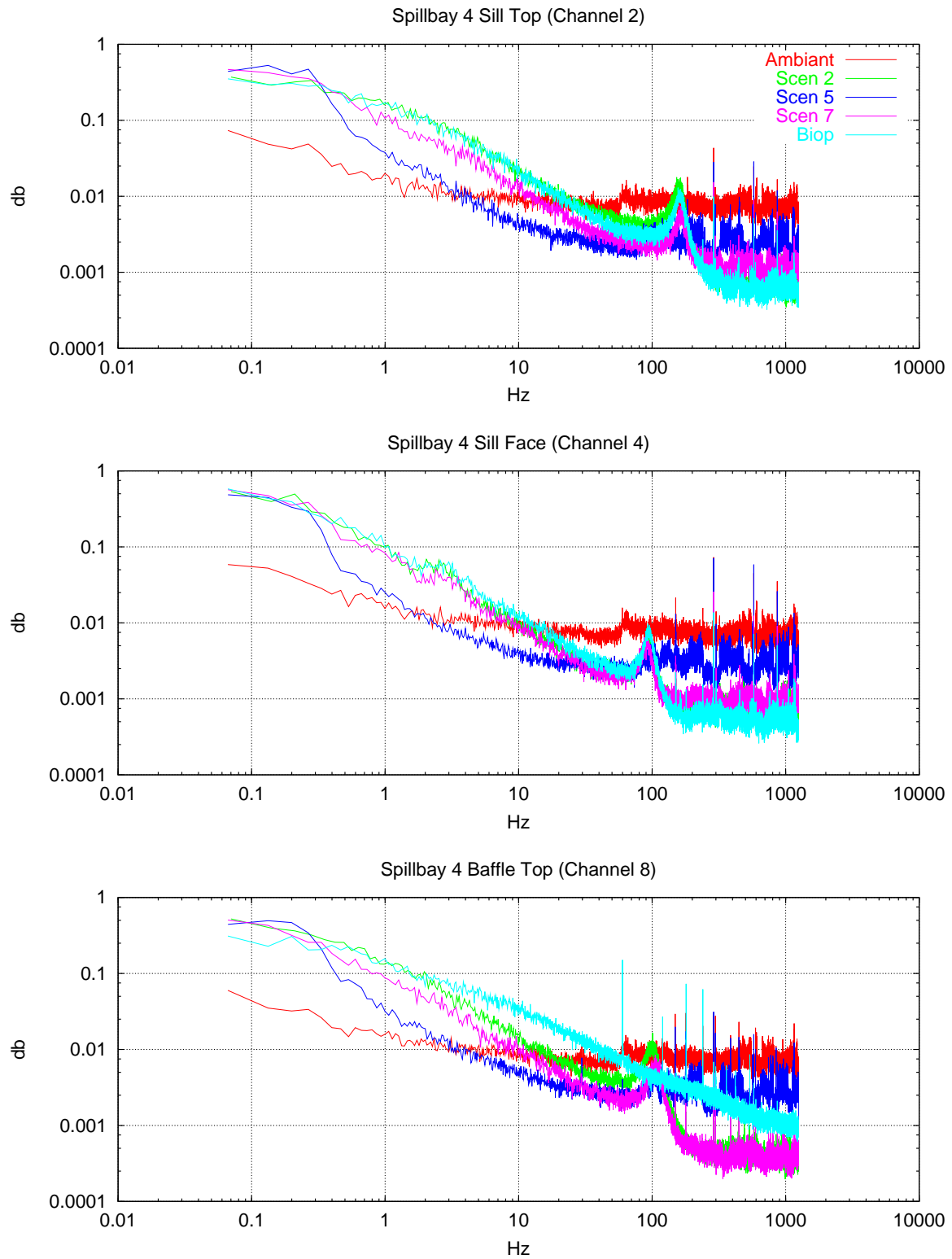


Figure A.2: Power spectra of static sensor data from spillbay 4

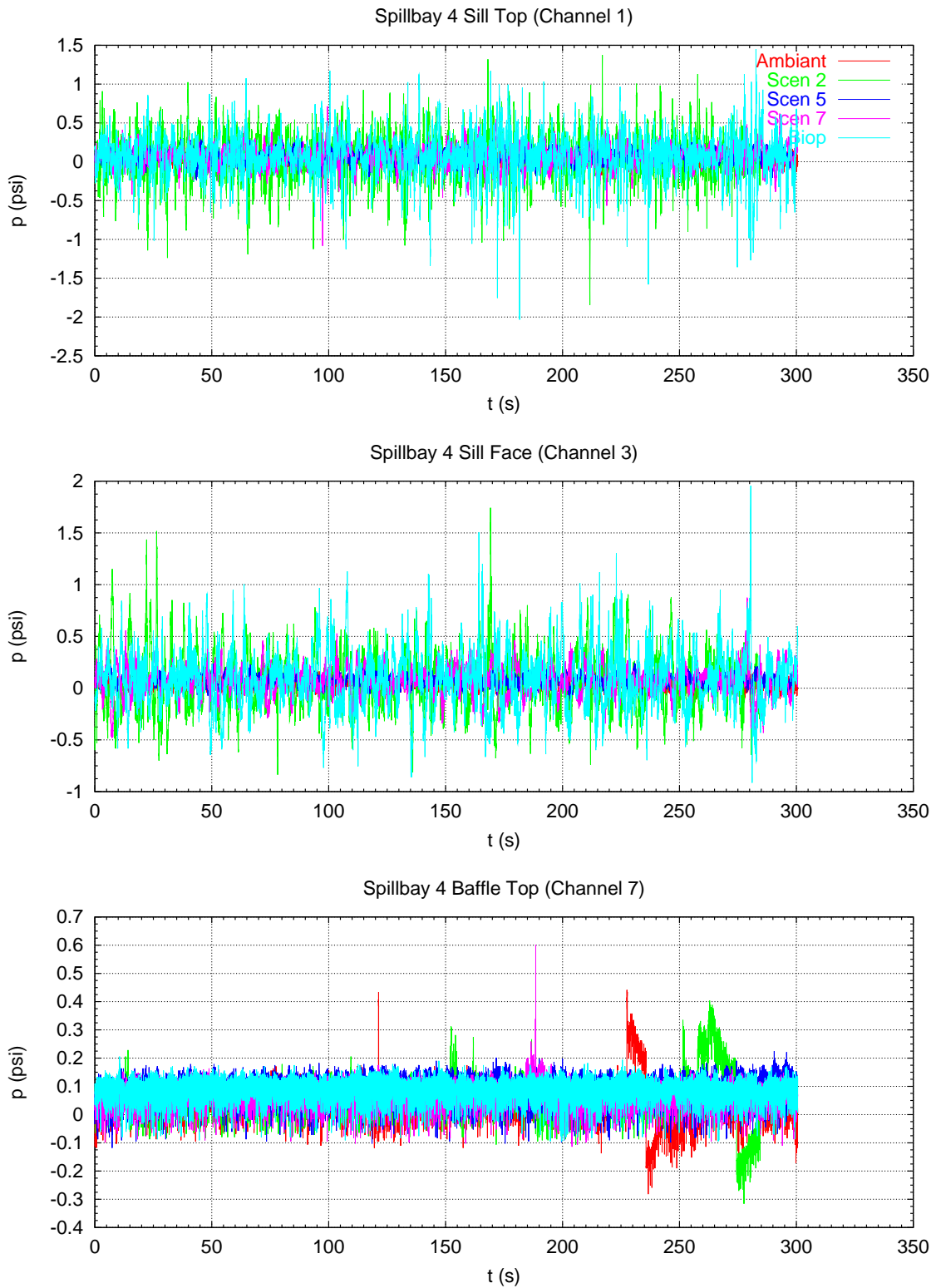


Figure A.3: Dynamic sensor data from spillbay 4

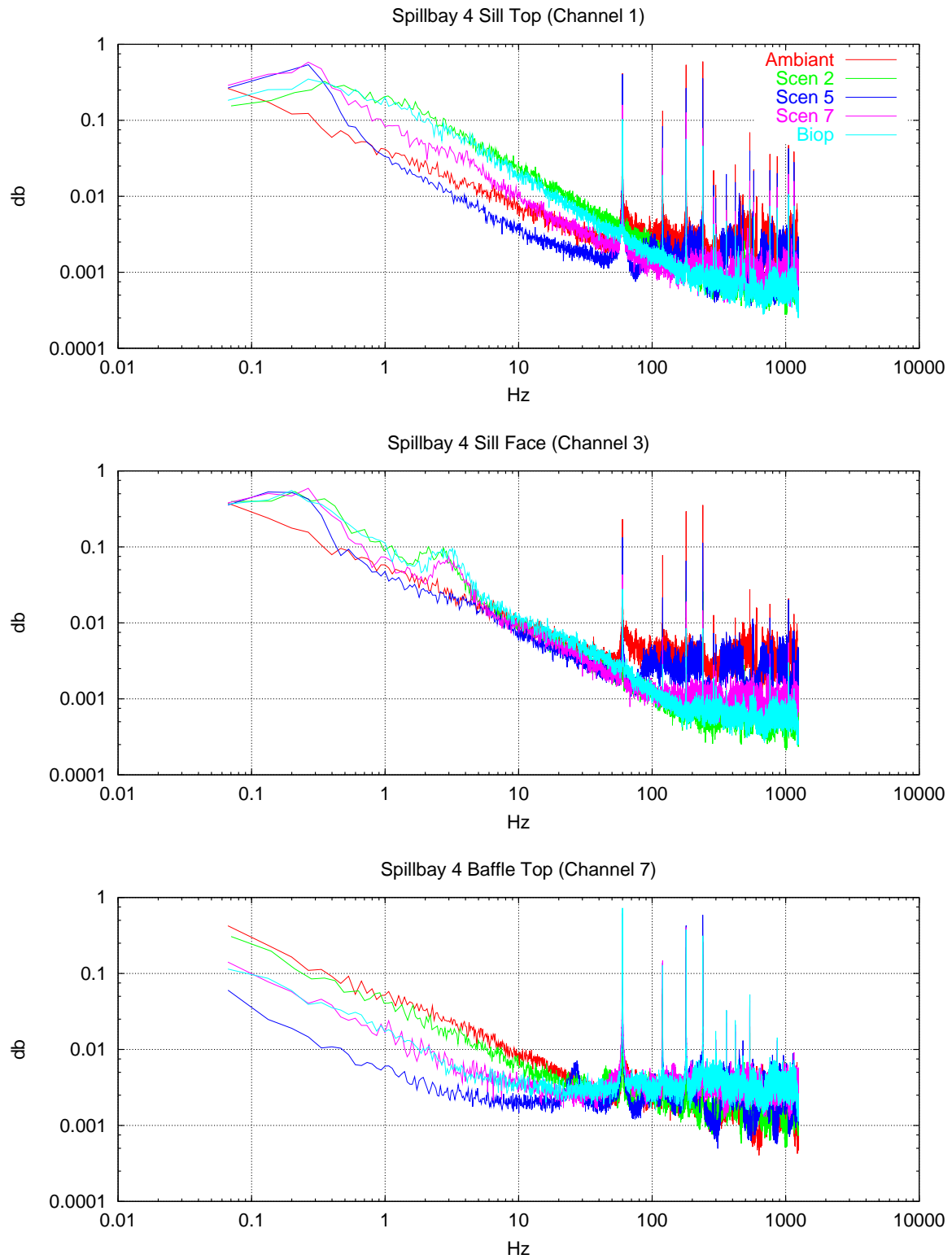


Figure A.4: Power spectra of dynamic sensor data from spillbay 4

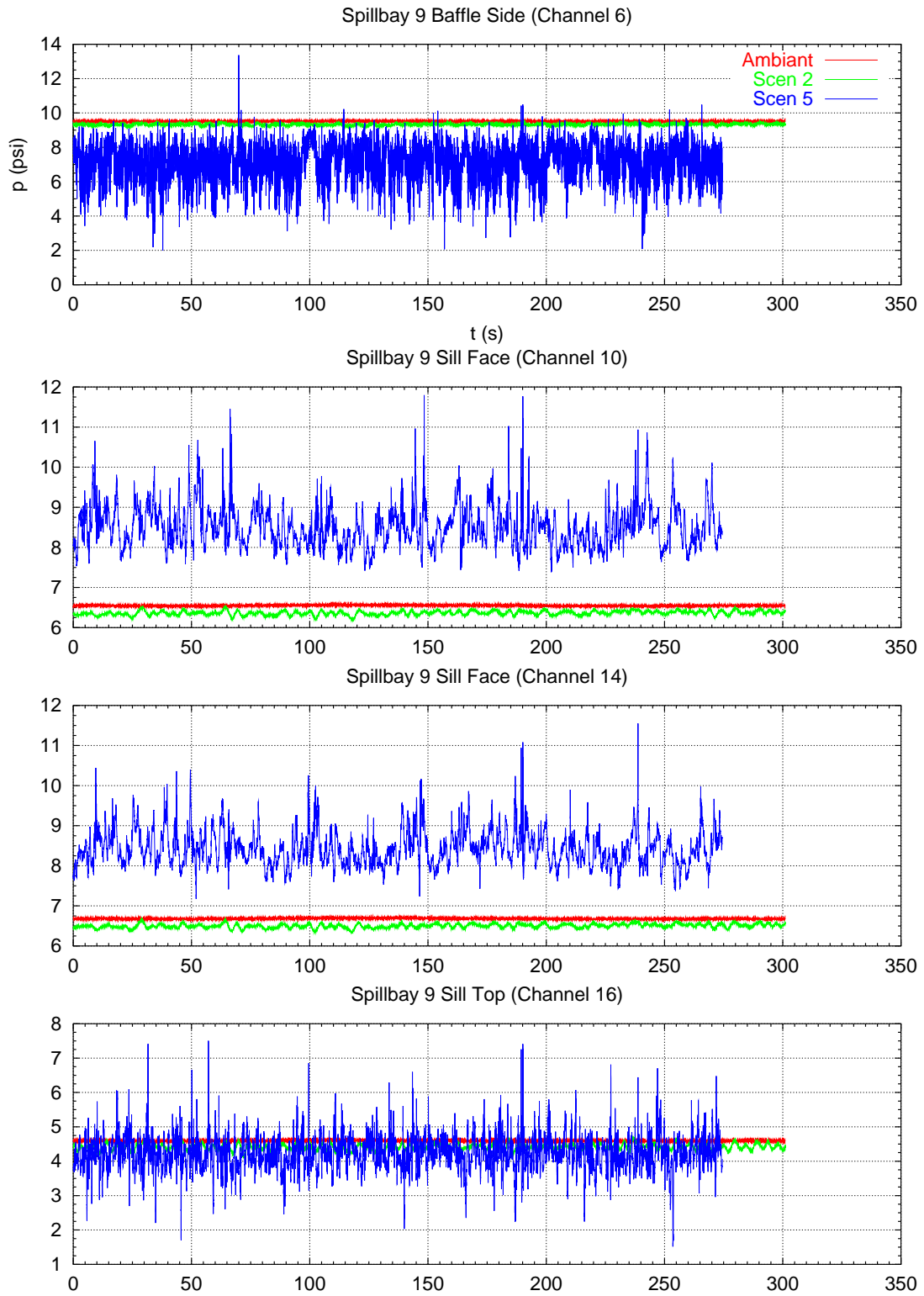


Figure A.5: Static sensor data from spillbay 9

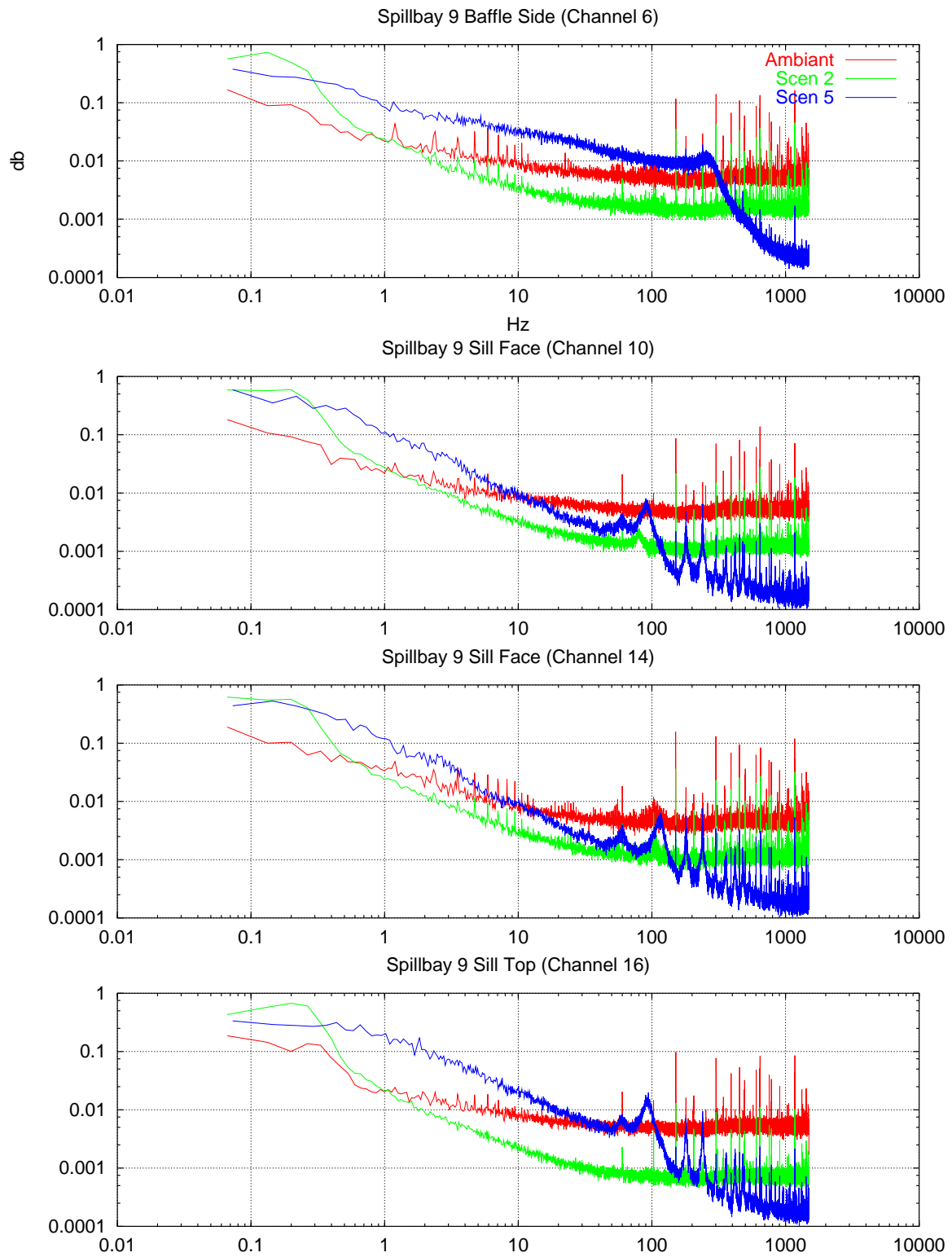


Figure A.6: Power spectra of static sensor data from spillbay 9